



Investigating small ion number size distributions: insight into cluster formation and growth

Santeri Tuovinen¹, Janne Lampilahti¹, Nina Sarnela¹, Chengfeng Liu¹, Yongchun Liu² and Markku Kulmala^{1,2} and Veli-Matti Kerminen¹

¹Institute for Atmospheric and Earth System Research/Physics, Faculty of Science, University of Helsinki, Helsinki, Finland

²Aerosol and Haze Laboratory, Beijing Advanced Innovation Center for Soft Matter Science and Engineering, Beijing University of Chemical Technology, Beijing, China

Correspondence: Santeri Tuovinen (santeri.tuovinen@helsinki.fi) and Markku Kulmala (markku.kulmala@helsinki.fi)

Abstract

Small ions, consisting mostly of charged molecular clusters with mobility diameters below 2 nm, exist continuously in the atmosphere. Here, we studied small ion number size distributions measured with Neutral cluster and Air Ion Spectrometer measurements in Hyytiälä, Finland and Beijing, China. We found that in Hyytiälä, there is a strong positive relationship between the concentration and diameter of small ions of both polarities and highly oxidized organic molecule (HOM) and sulfuric acid concentrations, and that the relationship with the former is especially strong. The relationship between the negative sulfuric acid cluster ions and the small ion number size distribution in Hyytiälä was found to be more complex, but overall positive. In contrast to Hyytiälä, we found that in Beijing the small ion number size distribution does not have a clear relationship with sulfuric acid or oxidized organic molecule (OOM) concentration. However, in both locations, the impact of growth on the small ion number size distribution during periods of intense cluster formation and new particle formation is clearly seen.

1 Introduction

Atmospheric aerosol particles influence the Earth's climate (e.g., Quaas et al., 2009; Boucher et al., 2013; Schmale et al., 2021; Li et al., 2022) and can have adverse effects on human health (e.g., Shiraiwa et al., 2017; Arfin et al., 2023). These influences have commonly been related to properties, such as the mass or number concentration of an atmospheric aerosol population, its size distribution, or its chemical composition (Shiraiwa et al., 2017; Atkinson et al., 2015; Finlay, 2021). The electric charging state of atmospheric aerosols has attracted much less interest, although this property may have large influences on the dynamics of atmospheric aerosol populations (Harrison and Carslaw, 2003; Fdez-Arroyabe et al., 2022), thereby affecting many other important aerosol properties. The presence of charges also makes it possible to measure low aerosol concentrations at high resolution in both time and particle size (Mirme and Mirme, 2013; Mirme et al., 2024).

Charged atmospheric particles, or more broadly ions, include charged aerosol particles, charged molecular clusters, and even large molecules having a charge. Ions with electrical mobility diameters roughly below 2 nm in diameter are classified as small ions, and consist of charged molecular clusters, while ions above 2 nm consist of charged aerosol particles (Tammet, 1995; Ehn



et al., 2010). Of these charged aerosol particles, those with diameters between 2 and 7 nm are referred to as intermediate ions (Tammet, 1995).

Atmospheric ions are created through ionization of molecules in the atmosphere. Most important of these ionization sources are cosmic ray radiation, gamma radiation, and radon decay (Harrison and Tammet, 2008). Small ions are constantly present in the troposphere as molecules are ionized and subsequently grow to small ions (Harrison and Tammet, 2008; Hirsikko et al., 2011). The lifetime of small ions is short at around 100 s, and their chemical composition depends on the atmospheric trace gas concentrations and their chemistry (Harrison and Tammet, 2008; Ehn et al., 2010; Shuman et al., 2015). In contrast, intermediate ions are typically detected mainly during the occurrence of atmospheric new particle formation (Tammet et al., 2014; Tuovinen et al., 2024), or during snowfall or rain (Hirsikko et al., 2007; Tammet et al., 2014). New particle formation (NPF) is considered to occur when constantly existing stable clusters, neutral or charged, start to grow to larger sizes by uptake of precursor vapors such as sulfuric acid and organic compounds with low volatilities (Kulmala et al., 2006; Kulmala et al., 2007; Lehtipalo et al., 2018; Kirkby et al., 2023).

A recent study by Kulmala et al. (2024a) presented the use of a novel cluster ion counter (CIC) for measuring small and intermediate ion concentrations to study local-scale NPF and to derive other parameters such as condensation sink (CS). The information gained by these measurements can be used further to study the complex climate-biosphere feedbacks (Kulmala et al., 2020; Kulmala et al., 2024b). These recent advances have motivated us to take a deeper look at the small ion size distribution.

The concentration of small ions depends on the ionization rate and the losses of small ions due to ion-ion recombination, coagulation with larger aerosol particles, and deposition (Tammet et al., 2006; Hörrak et al., 2008). The size of small ions depends on their chemical composition and age as the ions grow through chemical reactions and condensation of vapors, or through coagulation with neutral clusters. By investigating small ion number size distributions, we can learn more about these chemical and dynamical processes.

In this study, we combine ion number size distribution data measured by Neutral cluster and Air Ion Spectrometer (NAIS; Manninen et al., 2009; Mirme and Mirme, 2013) with concentrations of low-volatility vapors and ion clusters measured by mass spectrometer instruments to identify how, and why, the size distribution of small ions changes and evolves. Data from two different contrasting locations, Hyytiälä, Finland and Beijing, China (Kulmala et al., 2025), are used. First, we will study if the variation of the small ion size distribution with season is considerable. Secondly, we will quantify the potential relationship of organic low-volatility vapors and sulfuric acid on the size and number of small ions. Thirdly, we will analyze the small ion size distribution as a function of intensity of NPF to reveal how the small ion size distribution changes as the clusters grow. Finally, some case studies are presented. With these, we aim to identify the most important processes impacting the small ion number size distribution, and to evaluate the role of these processes in driving the growth of small ions to intermediate ions.



2 Background and methods

2.1 Evolution of small ion size distribution

Typically, the parameter of interest when considering small ions is their total number concentration and its temporal evolution. The changing in the small ion number concentration can be described by the simplified air ion balance equation:

$$\frac{dN^{\pm}}{dt} = Q - \text{CoagS} N^{\pm} - \alpha N^{\pm} N^{\mp} - S N^{\pm} \quad (1)$$

Here, N^{\pm} is the concentration of one polarity, while N^{\mp} is the concentration of the other polarity. The first term on the right-hand side of the equation describes the source rate of the ions, where Q is the ionization rate of air molecules. The second term, where CoagS stands for coagulation sink, tells the loss rate of small ions due to coagulation on larger aerosol particles. The third term tells the loss rate of ions due to ion-ion recombination, where α is the ion recombination coefficient. The final term describes other losses of the ions, including deposition, and S is the loss rate of the ions to these other sinks.

As we can see, the above equation does not explicitly depend on the size of the small ions nor can it be directly used to describe the evolution of the size-dependent small ion size distribution. The time evolution of small ions of certain size i are described by the charged general dynamics equations (charged GDEs; Kulmala et al., 2012):

$$\frac{dN_i^{\pm}}{dt} = J_i + \chi N_i N_{d < i}^{\pm} - N_i^{\pm} \text{CoagS}_i - \alpha N_i^{\pm} N_{d < i}^{\mp} - \frac{GR}{\Delta d_i} N_i^{\pm} \quad (2)$$

Here, J_i is the formation rates of ions of size i . The second term on the right-hand side represents the charging of neutral clusters by ions smaller than i , where χ is the ion-cluster attachment coefficient. The last term, where GR is the ion growth rate, describes the growth of ions i to larger sizes. Considering Eq. 2, we can see that an increasing GR will shift the ion size distribution towards larger diameters. CoagS is the highest for the smallest ions and if it increases, the concentrations of smallest ions are decreasing the most, causing an apparent shift in the distribution towards larger diameters. However, CoagS also affect the lifetime of small ions, so that with an increasing CoagS the ions have less time to grow, reducing the concentration of larger small ions. If ion concentrations are high, ion-ion recombination rate will be higher, which will also lead to shorter small ion lifetime and possibly smaller concentrations of larger small ions. Through ion-cluster attachment, the small ion size distribution depends on the size distribution of neutral clusters, although this term is relatively small when compared to the coagulation loss and growth terms. In this study, we are mainly interested in the formation and growth of ions, and their impacts on the small ion size distribution. Impacts of coagulation scavenging or ion-ion recombination on the small ion size distribution are not explicitly considered in this study.

2.2 Measurement sites

Two different locations were considered in this study: SMEAR II measurement station in Hyytiälä, Finland (61°51' N, 24°17' E) and BUCT/AHL measurement station in Beijing, China (39°94' N, 116°30' E). The former is a rural site surrounded by boreal forest while the latter is an urban site close to residential building and traffic roads. For more details on SMEAR II station, see Hari and Kulmala. (2005). For more details on BUCT/AHL site, see Liu et al. (2020). These two locations



are included in the analysis due to their contrasting natures, providing an opportunity for insight into the variation of small ion size distribution and small ion dynamics in different environments.

2.3 Measurement and other data

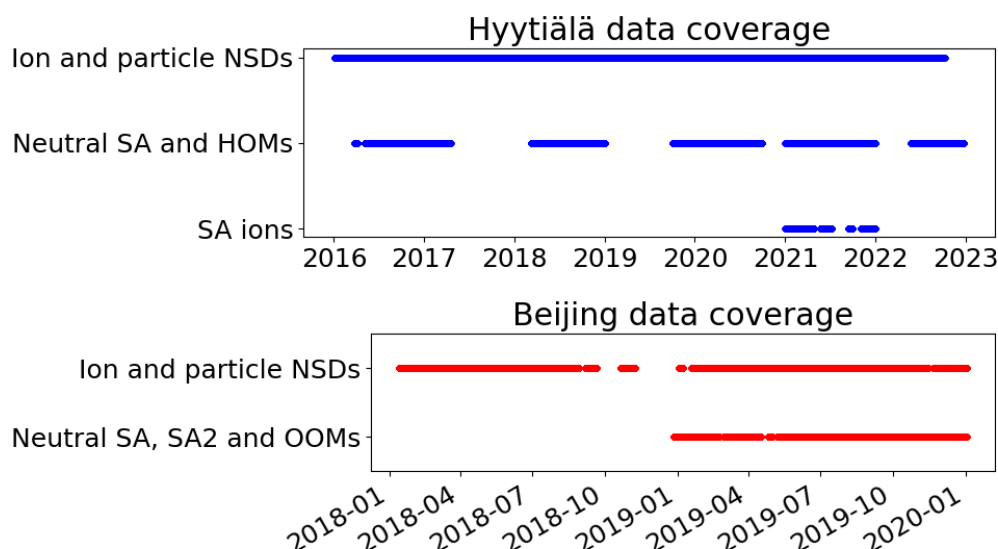


Fig.1: Data coverage for the two sites, Hyytiälä, Finland, and Beijing, China, from which data was used in this study. NSD refers to number size distribution, while SA refers to sulfuric acid, SA2 to neutral sulfuric acid dimer, HOM to highly oxidized organic molecule and OOM to oxidized organic molecule.

Atmospheric ion and total particle number size distributions in Hyytiälä and Beijing were measured with Neutral cluster and Air Ion Spectrometer (NAIS; Manninen et al., 2009; Mirme and Mirme, 2013). The NAIS measures both charged and total particle number size distributions in the ranges 0.8–42 nm and 2.5–42 nm, respectively. Main focus of the analysis in this study is on the number size distributions of small ions (diameters below 2 nm). Ion concentrations between 2.0 and 2.3 nm were used to characterize the intensity of local clustering (Tuovinen et al., 2023) and new particle formation ranking data, characterizing the intensity of NPF, was also used. The NPF ranking was based on the total particle number concentration between 2.5 and 5 nm and determined according to the method presented by Aliaga et al. (2023).

All diameters used in study are electrical mobility diameters. We note that especially for the smallest of the ions the mobility diameter may not accurately describe the physical dimensions of the ion (see e.g., Ehn et al., 2011). Regardless, we refer to diameter rather than electrical mobility as we see it as more intuitively understandable parameter for the ion size.

From Hyytiälä, concentrations of neutral sulfuric acid and highly oxidized organic molecules (HOMs) were used to study the influence of cluster formation and growth on the small ion size distribution. These were measured with Chemical Ionization Atmospheric Pressure interface Time-Of-Flight (CI-APi-TOF) mass spectrometer (Jokinen et al., 2012). In addition, the signal counts of ionized sulfuric acid clusters measured with APi-TOF were used to give further insight into the



composition of the small ions. The signal counts in the study are given as relative signals to the total measured ion current. From Beijing, neutral sulfuric acid, sulfuric acid dimer and total oxidized organic molecule (OOM) concentrations, which were measured with a nitrate based – long time-of-flight chemical ionization mass spectrometer (CIMS), were included in the analysis. We note that we use the term OOM instead of HOM for the organic molecules in Beijing based on previous results by Yan et al. (2021), suggesting that most of these measured organic molecules in Beijing do not meet the requirements for HOMs (see Bianchi et al., 2019).

Data coverage for both sites is presented in Fig. 1.

2.4 Determining the average small ion diameter

From the small ion number size distributions, we determined the mean mobility diameter (d_{mean}), and median mobility diameter (d_{median}) of small ions. First, cubic interpolation was applied to the measured ion number size distributions. We note that nearest neighbor and linear interpolation methods were also tested, and the influence of the chosen method on the value of d_{mean} or d_{median} was found minor. The diameter range for the interpolation was from the lower detection limit to 2 nm with a step of 0.001 nm. Then, d_{peak} was determined by finding the diameter corresponding to the maximum concentration of small ions. Weighted mean and median were used to determine d_{mean} and d_{median} , with the number concentrations of ions below 2 nm in diameter used as weights. The equation below was used to find weighted mean diameter:

$$d_{\text{mean}} = \frac{\sum N_i d_i}{\sum N_i}, \quad (3)$$

where d_i is the diameter of ions of a certain size and N_i is their number concentration. The weighted median was determined by finding the diameter d_j satisfying

$$j = \min_k \left[\sum N_i d_i > \frac{1}{2} \sum N_i d_i \right]. \quad (4)$$

3 Results

3.1 Seasonal variation of the small ion size distribution

3.1.1 Hyytiälä

The upper panel of Fig. 2 shows the monthly median negative and positive ion distributions between 0.8 and 2 nm in Hyytiälä. Table 2 records the monthly mean and median diameters (d_{mean} and d_{median}). Clear month-to-month changes in the size distributions are observed, and these are more pronounced for negative ions. During winter, the concentration of negative ions peaks already below 1 nm, while during summer the highest concentration is between 1.1 and 1.2 nm. In addition, the concentrations of negative ions above 1.1 nm are increased from winter to summer. Close to 2 nm, the ion concentration is almost one order of magnitude higher during summer. This behavior of the size distribution is reflected in the values of d_{mean} and d_{median} , which are smallest during December and January, with $d_{\text{mean}} = 0.99$ nm and $d_{\text{median}} = 0.95$ nm, and the largest during June and July, with $d_{\text{mean}} = 1.15$ nm and $d_{\text{median}} = 1.11$ nm.

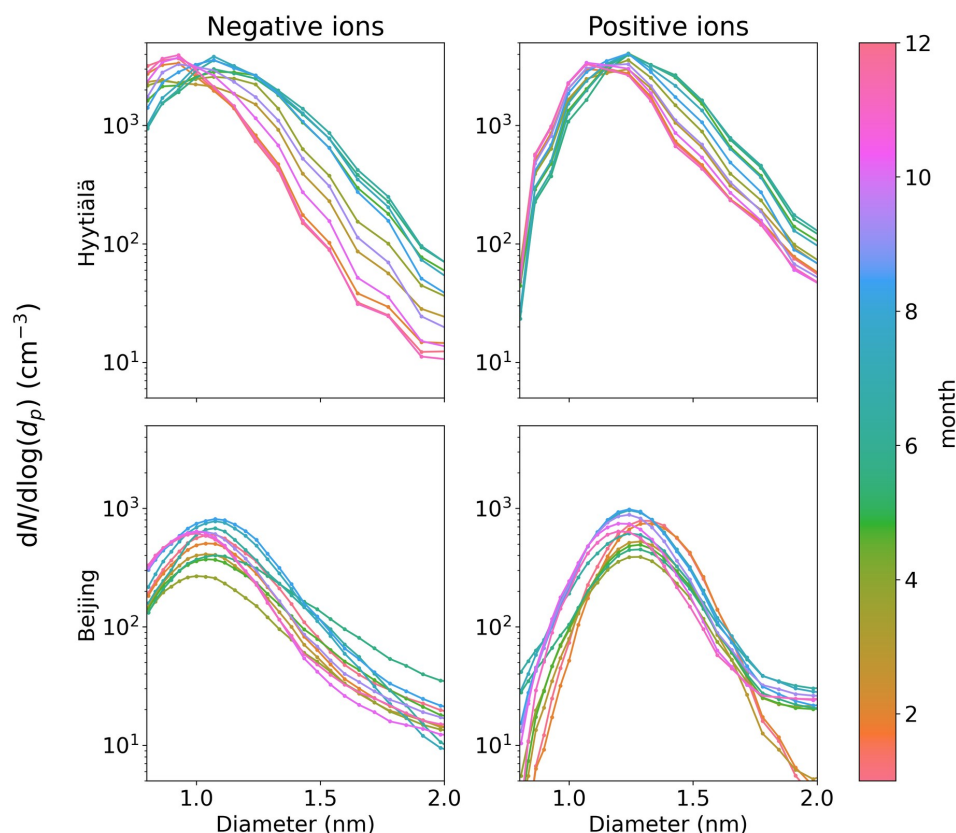
Positive ion size distributions behave similarly as the negative ones, however the changes are less pronounced. Above 1.4 nm and up to 2 nm, the concentrations are roughly twice as high, or less,



182 during summer compared to winter. For positive small ions, the smallest value of $d_{\text{mean}} = 1.16$ and
183 $d_{\text{median}} = 1.13$ nm (December and January) and the largest value of $d_{\text{mean}} = 1.29$ nm and $d_{\text{median}} = 1.27$
184 nm (June). The difference between the average diameters of negative and positive small ions was
185 around 0.15 nm, in line with previous studies (e.g., Hörrak et al., 2000).

186 The observed seasonal behavior of the size distributions in Hyytiälä follow expectations: during
187 spring and summer, the concentrations of low-volatility vapors are much higher due to increased
188 solar radiation and organic emissions (Sulo et al., 2021). Therefore, small ions should be able to
189 grow to larger diameters due to the uptake of these vapors. We will look further into how the small
190 ion size distribution varies with respect to low volatile vapor concentrations in Sect. 3.2.

191 3.1.2 Beijing



192
193 **Fig. 2:** Median monthly sub-2 nm negative (left) and positive (right) ion size distributions for
194 Hyytiälä (top) and Beijing (bottom). The different months are marked by different colors.

195
196 The bottom panel of Fig. 2 shows the monthly median negative and positive ion distributions
197 between 0.8 and 2 nm in Beijing, while Table 3 records the monthly d_{mean} and d_{median} . Compared to
198 Hyytiälä, the seasonal trends in Beijing are much more unclear and complex. For negative ions, the
199 concentrations during summer are higher than in other seasons below 1.6 nm and lower than in
200 other seasons close to 2 nm. During spring, the concentrations of negative ions below 1.4 nm are



201 lower than in other seasons. The smallest value of negative d_{mean} and d_{median} are in November, $d_{\text{mean}} =$
202 1.04 nm and $d_{\text{median}} = 1.01$ nm. The largest values are during June, $d_{\text{mean}} = 1.16$ nm and $d_{\text{median}} = 1.12$
203 nm.

204 For positive small ions in Beijing, the concentrations of ions close to 0.8 nm and 2 nm are both
205 considerably lower from January to March compared to later months. Otherwise, it is difficult to
206 identify any clear patterns. The largest positive average diameter is during February, $d_{\text{mean}} = 1.32$ nm
207 and $d_{\text{median}} = 1.31$ nm, while the smallest values are in November, $d_{\text{mean}} = 1.22$ nm and $d_{\text{median}} = 1.21$
208 nm.

209 We note that because there are less data from Beijing compared to Hyytiälä, variation between years
210 can have larger impact on the results than in Hyytiälä.

211

212 **Table 1:** Mean and median monthly diameters (nm) of ions between 0.8 and 2 nm in Hyytiälä. *The
213 highest concentration corresponds to the lowest detected diameter.

	Negative ions		Positive ions	
Month	d_{mean}	d_{median}	d_{mean}	d_{median}
1	0.99	0.95	1.16	1.13
2	1.00	0.96	1.17	1.15
3	1.05	1.02	1.2	1.18
4	1.08	1.06	1.21	1.20
5	1.12	1.10	1.27	1.25
6	1.15	1.11	1.29	1.27
7	1.15	1.11	1.28	1.26
8	1.13	1.10	1.25	1.23
9	1.11	1.08	1.22	1.20
10	1.05	1.02	1.19	1.17
11	1.01	0.98	1.17	1.14
12	0.99	0.95	1.16	1.13

214

215

216 **Table 2:** Mean and median monthly diameters (nm) of ions between 0.8 and 2 nm in Beijing. *The
217 highest concentration corresponds to the lowest detected diameter.

	Negative ions		Positive ions	
Month	d_{mean}	d_{median}	d_{mean}	d_{median}
1	1.10	1.07	1.30	1.30
2	1.09	1.06	1.32	1.31
3	1.09	1.06	1.28	1.27
4	1.10	1.05	1.28	1.26



5	1.12	1.07	1.28	1.27
6	1.16	1.12	1.27	1.26
7	1.12	1.08	1.25	1.24
8	1.10	1.08	1.25	1.24
9	1.10	1.07	1.25	1.24
10	1.07	1.03	1.24	1.23
11	1.04	1.01	1.22	1.21
12	1.05	1.01	1.23	1.21

218

219 **3.2 Potential impact of low volatility vapors to small ion size distribution** 220 **in Hyytiälä**

221 **3.2.1 highly oxidized organic molecules (HOMs)**

222 Fig. 3 shows the median ion number size distributions between 0.8 and 2 nm in Hyytiälä with
 223 respect to varying neutral highly oxidized organic molecule (HOM) concentration. HOM
 224 monomers, HOM dimers and total HOM are considered separately. Results for daytime (10:00-
 225 16:00) and evening (18:00-00:00) are both presented (Fig. 3a and 3b, respectively). The HOM
 226 concentrations are divided into percentiles.

227 A clear increase in the number of negative ions above approx. 1.05 nm, and for positive ions
 228 slightly larger than that, is seen with an increasing HOM concentration percentile for all the plotted
 229 HOM categories. The difference is largest for HOM monomers and HOM total, which is mainly
 230 dominated by the HOM monomers. The difference is also stronger for negative ions than positive
 231 ions, and is stronger during the evening (Fig. 3b) compared to daytime (Fig. 3a).

232 Comparing the negative ion size distributions between the HOM percentiles of 0-20% and 80-
 233 100%, we see that the difference in the concentrations increases with an increasing diameter, and
 234 that close to 2 nm this difference is approximately one order of magnitude during daytime (Fig. 3a)
 235 and a bit more than that during the evening (Fig. 3b). The negative ion size distributions for
 236 different HOM percentiles are otherwise quite similar during the daytime and evening, however
 237 during the evening the difference between the respective size distributions for HOM monomer
 238 percentile 60-80% and 80-100% is higher (Fig. 3b). During daytime, the ion concentrations are
 239 similar in the 60-80% and 80-100% percentiles (Fig. 3a), while during the evening, the
 240 concentration close to 2 nm is around twice as high when HOM monomer concentration is in the
 241 80-100% percentile compared to 60-80% percentile (Fig. 3b). Comparing similar negative ion
 242 concentrations when HOM monomer concentration during the evening is in the 80-100% percentile
 243 compared to 0-20%, there's approx. a 0.5 nm shift in diameters, a major difference for the sub-2 nm
 244 ion population.

245 In line with the large differences in the small ion size distributions in Fig. 3 with respect to HOM
 246 concentration, a strong correlation between the small ion d_{mean} and the HOM concentrations was
 247 seen (Fig. 4). The Spearman correlation coefficients (r_s) between d_{mean} and HOMs were 0.6 or
 248 above, for both daytime and evening. For daytime, the best correlation was between d_{mean} of positive



249 ions and HOM monomer concentration, $r_s = 0.74$. During nighttime, the strongest correlation was
250 between d_{mean} of negative ions and HOM monomer concentration, $r_s = 0.73$. By using a variable
251 such as d_{mean} , we have been able to get some insight about the behavior of the underlying ion size
252 distribution.

253 The clear correlation between HOMs and the small ion size distribution in Hyytiälä suggests a
254 strong impact of organic compounds to the small ion population. This interpretation, as opposed to
255 the correlation being due to a correlation with another variable such as sulfuric acid concentration, is
256 supported by the observation of the correlation being stronger during evening when the
257 concentrations of other precursors such as sulfuric acid are lower and organic ion cluster formation
258 is known to take place in Hyytiälä (Mazon et al., 2016; Rose et al., 2018). Part of the increase in
259 diameters of small ions when HOMs are abundant could be due to the large size of organic
260 molecules when compared to sulfuric acid molecules. However, the clear increase in concentrations
261 even close to 2 nm suggests that a significant part of the impact is due to the growth of small ions
262 by uptake of organic vapors.

263 While the concentrations of larger small ions of both polarities increase with increasing HOM
264 percentile, the differences are larger for the negative ions (Fig. 3). This could be due to the uptake
265 of organics being more effective for negatively charged ions. However, the equally strong
266 correlation between d_{mean} of positive small ions and HOM concentrations does not support this
267 interpretation. A possible explanation is the size difference between the negative and positive small
268 ions: due to the larger diameter of positive small ions, it might be that the impact of the growth to
269 the diameters of the positive ions is not as large. For a larger cluster (ion), more molecules are
270 needed to increase the diameter equally than for a smaller one.

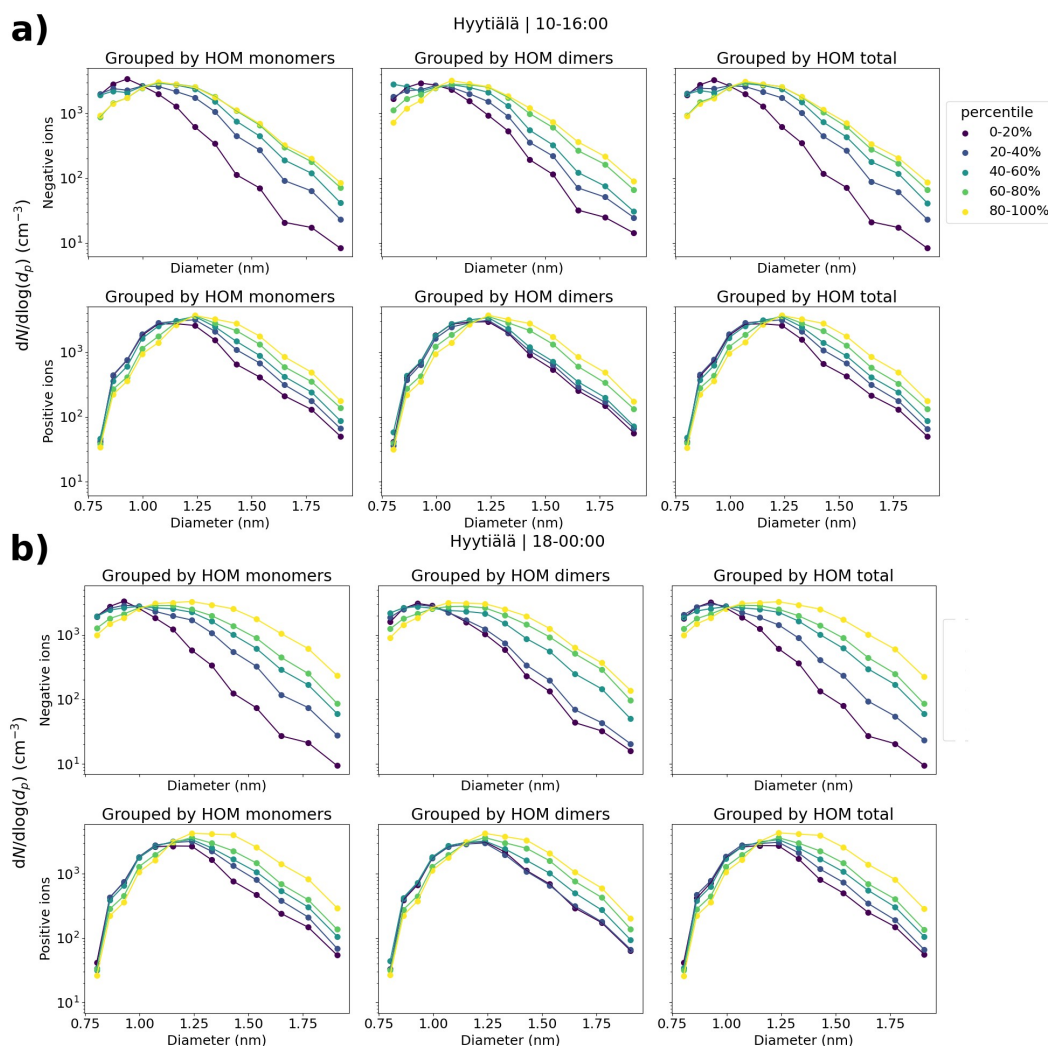


Fig. 3: The median negative and positive small ion (sub-2 nm) size distributions in Hyytiälä, Finland grouped by the percentiles of neutral HOM monomer, HOM dimer and total HOM concentrations. Both the evening (18:00-00:00) size distributions (b) and daytime (10:00-16:00) size distributions (a) are shown. Daytime percentiles for HOM monomers, dimers and total are 20%: $4.30 \cdot 10^6$, $5.93 \cdot 10^5$, and $5.10 \cdot 10^6$ cm^{-3} ; 40%: $1.34 \cdot 10^7$, $1.45 \cdot 10^6$, and $1.50 \cdot 10^7$ cm^{-3} ; 60%: $4.00 \cdot 10^7$, $2.44 \cdot 10^6$, and $4.18 \cdot 10^7$ cm^{-3} ; 80%: $9.70 \cdot 10^7$, $7.62 \cdot 10^6$, and $1.05 \cdot 10^8$ cm^{-3} , respectively. Evening percentiles for HOM monomers, dimers and total are 20%: $3.00 \cdot 10^6$, $4.94 \cdot 10^5$, and $3.75 \cdot 10^6$ cm^{-3} ; 40%: $8.40 \cdot 10^6$, $1.50 \cdot 10^6$, and $1.03 \cdot 10^7$ cm^{-3} ; 60%: $3.17 \cdot 10^7$, $2.95 \cdot 10^6$, and $3.65 \cdot 10^7$ cm^{-3} ; 80%: $7.52 \cdot 10^7$, $7.70 \cdot 10^6$, and $8.46 \cdot 10^7$ cm^{-3} , respectively.

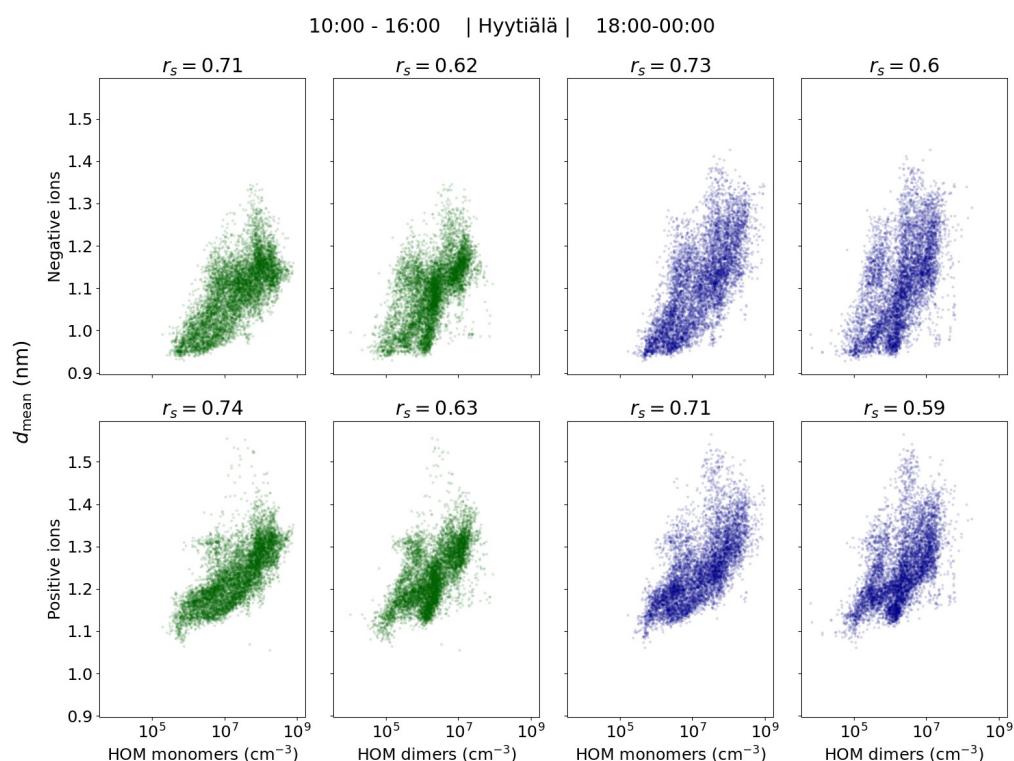


Fig. 4: Mean diameter (d_{mean}) of positive and negative small (sub-2 nm) ions as a function of HOM (monomer, dimer and total) concentration in Hyytiälä. The individual points are hourly medians, and the daytime (10:00-16:00, marked in green) and evening (18:00-00:00, marked in dark blue) are shown separately. Spearman correlation coefficients (r_s) are shown.

3.2.2 Sulfuric acid

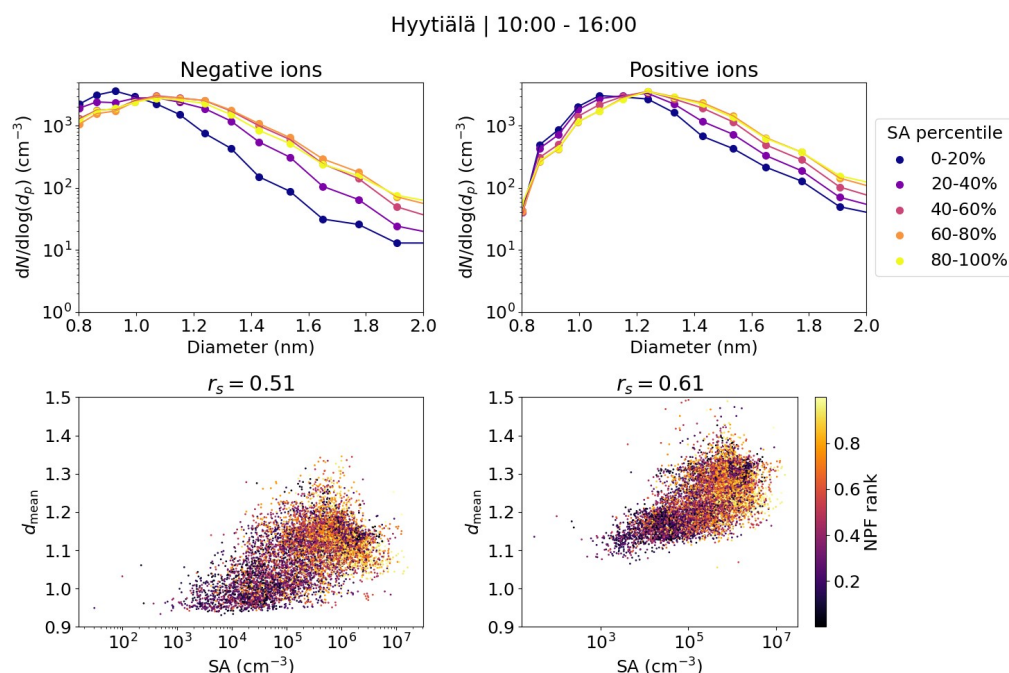
Fig. 5 shows the median daytime negative and positive small ion (0.8-2 nm) size distributions grouped by percentiles of neutral sulfuric acid (SA) concentration, add percentiles here. In addition, the daytime hourly median d_{mean} values are shown as a function of the SA concentration. We see a clear increase in the concentrations of negative (positive) small ions larger than approximately 1.05 (1.1) nm when comparing SA concentrations in the lower percentiles to the higher percentiles, until the behavior seems to stall so that the 60-80% and 80-100% percentiles show similar size distributions. From previous studies, we know that while sulfuric acid is often needed for the initial cluster formation, organic compounds tend drive cluster growth (Kulmala et al., 2013). This might partially explain the small difference in the size distributions between the 60-80% and 80-100% percentiles of the SA concentration.

A good positive correlation was seen between d_{mean} and SA concentration for both polarities, $r_s = 0.51$ (0.61) for negative (positive) ions (Fig. 5). The correlation is slightly weaker than was observed between d_{mean} and HOM, especially monomer, concentrations. The majority of d_{mean} values above 1.1 nm correspond to days with high NPF ranking, while most values of d_{mean} below 1.1 nm correspond to days with low NPF rank values below 0.5. Notably, for d_{mean} of negative small ions



above approx. 1.1 nm, the values of d_{mean} do not seem to increase with an increasing SA concentration as clearly as they do with increasing HOM concentration (Fig. 4). As discussed above, organic compounds might be needed to drive the growth of small ions further, and thus dependency of d_{mean} on SA is not seen as clearly when d_{mean} is above 1.1 nm.

308



309

Fig. 5: The median number size distributions of small ions between 0.8 and 2 nm grouped by percentiles of neutral sulfuric acid concentration (percentiles; top panel) and scatter plot and Spearman correlation coefficients (r_s) of hourly mean diameter of small ions (d_{mean}) and sulfuric acid concentration (bottom panel) in Hyytiälä. In the scatter plot, the color indicates the respective NPF rank of the day. Only daytime (10:00-16:00) values are included. The percentile values for sulfuric acid are 20%: $4.22 \cdot 10^4 \text{ cm}^{-3}$, 40%: $1.79 \cdot 10^5 \text{ cm}^{-3}$, 60%: $5.06 \cdot 10^5 \text{ cm}^{-3}$ and 80%: $1.08 \cdot 10^6 \text{ cm}^{-3}$.

315



3.3 Relationship of small ion size distribution with low volatility vapors in Beijing

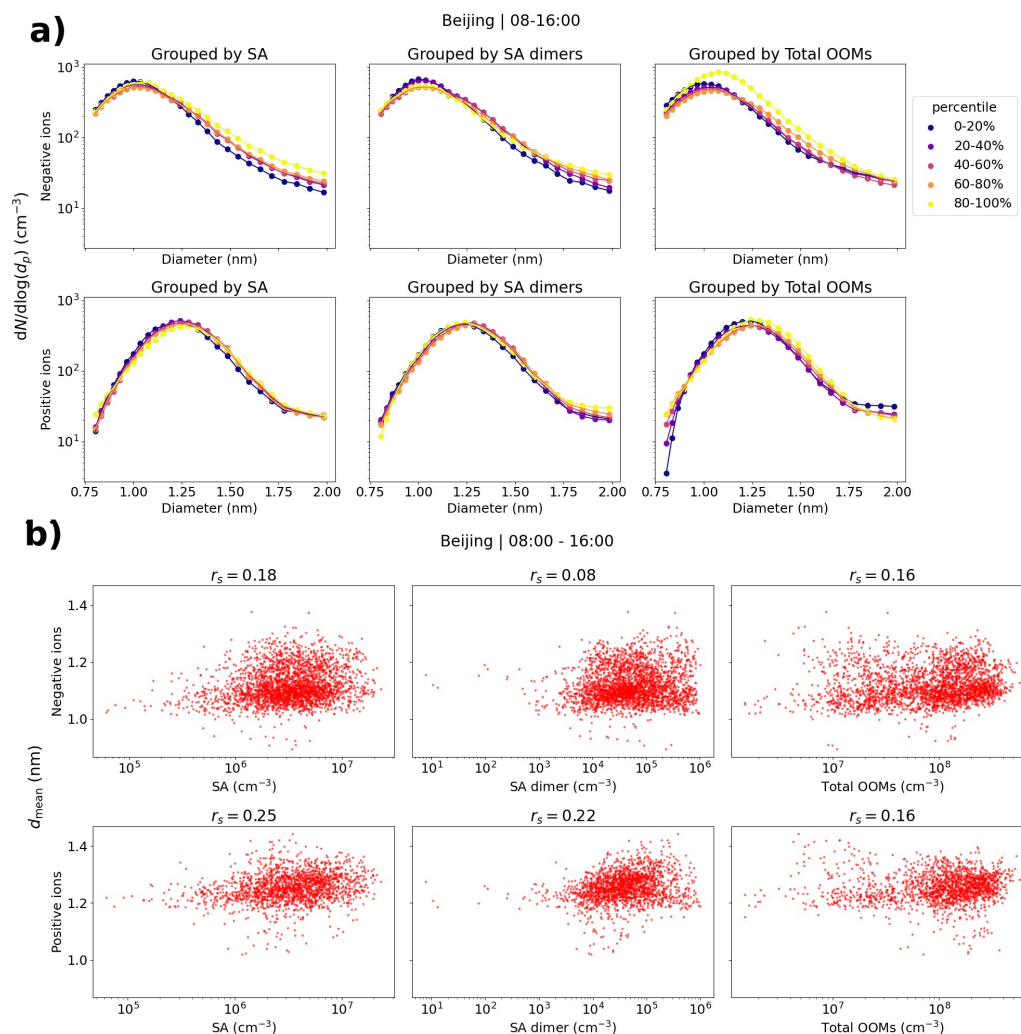


Fig. 6: (a) Small ion median daytime (08:00-16:00) number size distributions in Beijing, grouped by percentiles of sulfuric acid (SA), SA dimer or total oxidized organic molecule (OOM) concentrations. (b) Hourly daytime mean diameter (d_{mean}) of small ions versus SA, SA dimer and total OOM concentrations. Spearman correlation coefficients (r_s) are included. The percentile limits of SA, SA dimer and total OOM are 20%: $1.64 \cdot 10^6$, $1.26 \cdot 10^4$, and $2.19 \cdot 10^7 \text{ cm}^{-3}$; 40%: $2.53 \cdot 10^6$, $3.11 \cdot 10^4$, and $5.89 \cdot 10^7 \text{ cm}^{-3}$; 60%: $3.66 \cdot 10^6$, $6.01 \cdot 10^4$ and $1.23 \cdot 10^8 \text{ cm}^{-3}$; and 80%: $5.17 \cdot 10^6$, $1.32 \cdot 10^5$, and $2.15 \cdot 10^8 \text{ cm}^{-3}$.

Fig. 6a shows the number size distributions of small ions grouped by percentiles of neutral sulfuric acid, sulfuric acid dimer and total oxidized organic molecule (OOM) concentration in Beijing. We can see that, especially compared to results already for Hyytiälä, the differences in the size distributions are small for either polarity. The concentration of negative ions below approx. 1.2 nm



slightly decreases with increasing sulfuric acid and sulfuric acid dimer concentration, while the concentrations above approx. 1.2 nm increase. Close to 2 nm, where the increase is the highest, the concentration of ions is higher by around a factor of two when sulfuric acid concentration is in the 80-100% percentile compared to when it is in the 0-20% percentile. For both polarities, the concentrations below approx. 1.75 nm appear higher when total OOM concentration is in the 80-100% percentile compared to other times. However, the concentrations close 2 nm are not simultaneously higher, indicating that despite the increased concentration of small ions, more of them are not growing to intermediate ions.

Fig. 6b shows the scatter plots of d_{mean} and sulfuric acid, sulfuric acid dimer and total OOM concentrations. Weak positive correlation is seen, and the Spearman correlation coefficients (r_s) are between 0.08 and 0.25. The differences in the values of d_{mean} are small. The relationship between the small ion size distribution or d_{mean} and low volatility vapor concentrations in Beijing appears weak and much less clear compared to Hyytiälä. Due to the high concentration of both low volatility vapors and large particles, the dynamics of small ions in a megacity such as Beijing are different than in a rural site such as Hyytiälä.

3.4 Correlation of small ion size distribution with sulfuric acid clusters and NPF in Hyytiälä

Fig. 7a shows the median number size distribution of negative small ions grouped by percentiles of the signals of SA ion clusters HSO_4^- (monomer), $\text{H}_2\text{SO}_4\cdot\text{HSO}_4^-$ (dimer) and $(\text{H}_2\text{SO}_4)_2\cdot\text{HSO}_4^-$ (trimer) and their ratios in Hyytiälä. The median distributions are determined from daytime (10:00-16:00) values with clear sky conditions. We observe a clear increase in the number of small ions with diameters above approx. 1.2 nm with the increased signal of SA ion monomers and dimers. The increase is especially clear for dimers and the dimer to monomer ratio, and the concentration of small ions close 2 nm, where the differences are highest, is an order of magnitude higher when dimer signal is in the 80-100% percentile compared to when the signal is in the 0-20% percentile. These results indicate that the dimer signal is a strong indicator for the cluster formation and the growth of clusters to larger sizes in Hyytiälä.

Fig. 7b shows the median daytime (10:00-16:00) size distributions for both polarities with respect to the percentiles of 2.0-2.3 nm ion concentrations and bins of NPF ranking (Aliaga et al., 2023) in Hyytiälä. When the 2.0-2.3 nm ion concentration is higher, a clear increase in concentrations is seen above approx. 1.2 nm. The difference in negative small ion concentrations close to 2 nm between 80-100% and 0-20% is over one order of magnitude. A high 2.0-2.3 nm ion concentration indicates intense local-scale cluster formation and NPF (Tuovinen et al., 2024), and we can see from the small ion size distribution for both polarities how this growth of small ions up to 2.0 nm is seen in the small ion population as an increase in the concentrations of larger small ions.

Similar observations can be made from the small ion size distributions with respect to the different NPF ranking values. However, the differences are smaller than with respect to 2.0-2.3 nm ions, and especially for positive small ions such differences are very small. There is likely a combination of factors at play here. First of all, NPF ranking was determined for total particles between 2.5 and 5 nm and there might be differences stemming both from the ranking being less sensitive for local NPF and for 2.0-2.3 nm ion concentrations being more sensitive for ion-induced clustering or NPF.

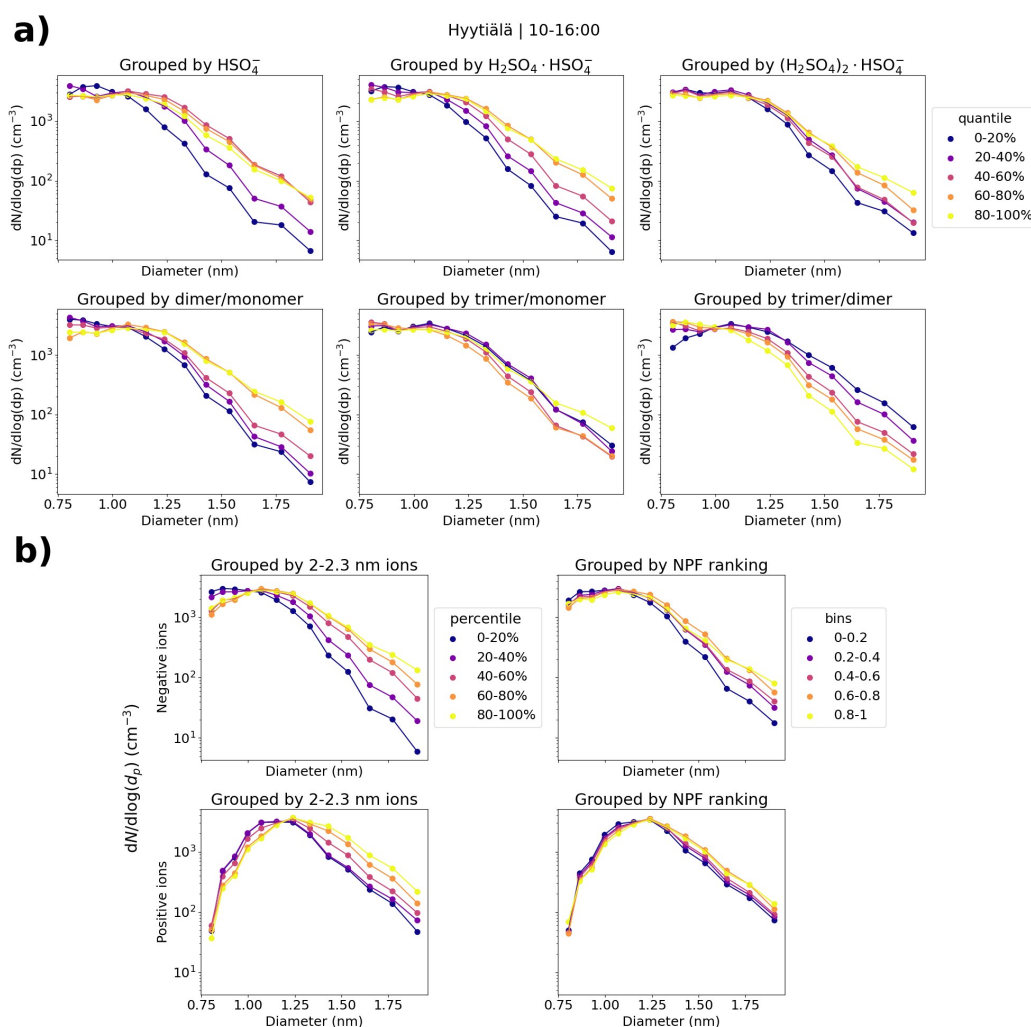


371 In addition, differences between what is observed in the total particles versus ions can be caused by
372 variation in the chemical compounds, which take up the available charges (Bianchi et al., 2017).

373 We note that the differences in the number size distribution of positive small ions are once again
374 smaller than for negative small ions. Similarly to Sect. 3.2.1, we hypothesize that this is due to the
375 size difference between the polarities.

376 Fig. 8 shows the scatter plot of hourly daytime small ion d_{mean} and the concentration of 2.0-2.3 nm
377 ions. As expected, a strong positive trend is seen between d_{mean} and 2.0-2.3 nm ion concentrations.
378 The correlation coefficient is $r_s = 0.54$ (0.67) for negative (positive) ions. Fig. 8 also shows the box
379 plots of d_{mean} with NPF ranking. The median of d_{mean} increases with increasing NPF ranking, as
380 expected. However, the variance for lower rankings is much higher, resulting in overall quite a low
381 correlation between d_{mean} and NPF ranking, $r_s =$ for negative (positive small) ions.

382

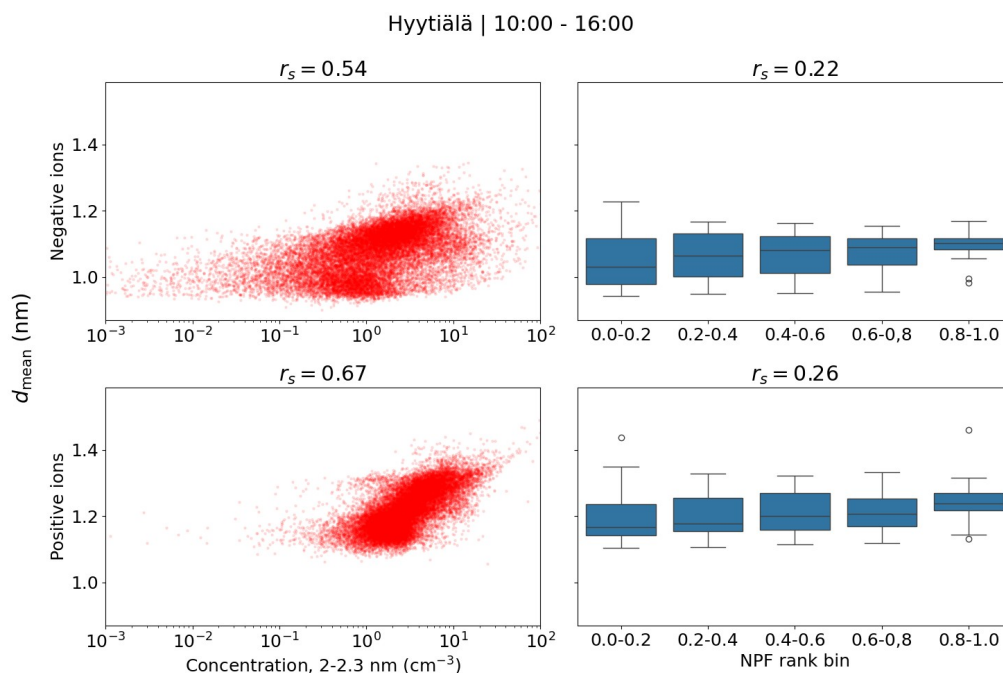


383



Fig. 7: (a) Hyytiälä daytime median negative small ion number size distributions grouped by percentile of the signals of HSO_4^- , $\text{H}_2\text{SO}_4\cdot\text{HSO}_4^-$ or $(\text{H}_2\text{SO}_4)_2\cdot\text{HSO}_4^-$ ions and their ratios. (b) Daytime median small ion size distributions for both polarities grouped by the percentile of 2.0-2.3 nm ion concentrations of the respective polarity or by NPF ranking. The percentile limits for negative (positive) 2.0-2.3 nm ion concentrations are 20%: 0.48 (1.75) cm^{-3} , 40%: 1.01 (2.34) cm^{-3} , 60%: 1.94 (3.49) cm^{-3} , and 80%: 3.39 (5.35) cm^{-3} .

390
391



392

Fig. 8: Hourly daytime negative and positive small ion diameter versus concentration of 2.0-2.3 nm ions of respective polarity or NPF ranking in Hyytiälä. Correlation coefficients (r_s) are also shown. The middle line of the box plots for d_{mean} and NPF rank are the median values, while the boxes show the 25% and 75% percentiles and the lines the 10% and 90% percentiles.

396

397

398



399 3.5 Impact of NPF on small ion distribution in Beijing

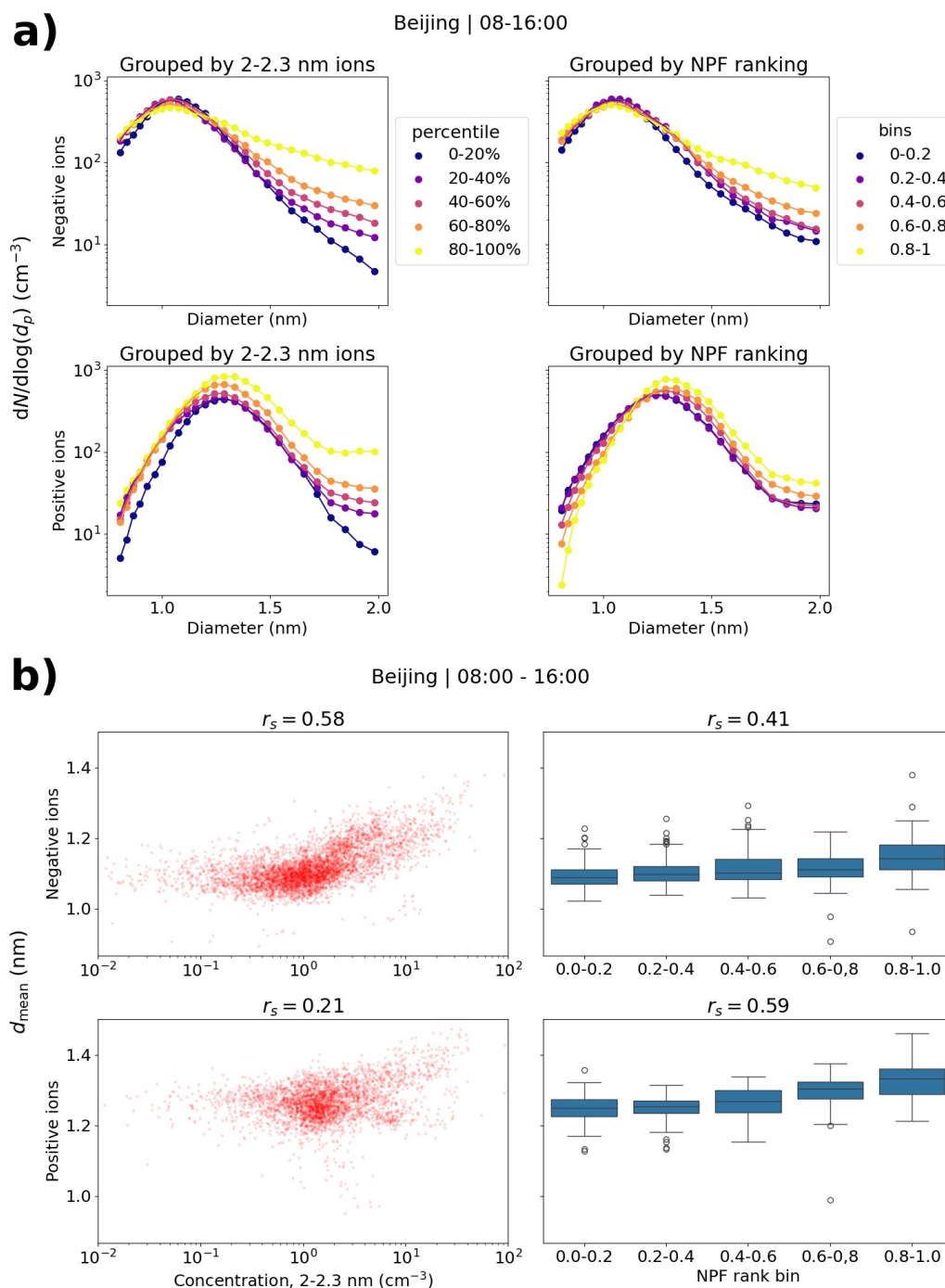


Fig. 9: (a) Median negative and positive small ion number size distributions in Beijing grouped by percentiles of 2.0-2.3 nm ion concentrations (of respective polarity) or by NPF ranking. (b). Scatter



plots of mean diameter and 2.0-2.3 nm ion concentrations (of respective polarity) or NPF ranking. Values are for daytime (08:00-16:00). The percentile limits of 2.0-2.3 nm concentration for negative (positive) ions are 20%: 0.51 (0.85) cm^{-3} , 40%: 0.92 (1.27) cm^{-3} , 60%: 1.33 (1.72) cm^{-3} , and 80%: 2.47 (3.22) cm^{-3} .

Fig. 9a shows the small ion size distributions with respect to the concentration of 2.0-2.3 nm ions or NPF ranking in Beijing. For both polarities, clear differences are seen in the distributions depending on the percentile of the 2.0-2.3 nm ion concentration. When the 2.0-2.3 nm ion concentrations are higher, the concentration of negative (positive) small ions above approx. 1.0 (1.3) nm is increased. Relative to the concentrations, the differences are largest close to 2 nm. Comparing the 0-20% and 80-100% percentiles, the difference in concentrations is around one order of magnitude when the diameter is approaching 2 nm. Similar observations are seen with respect to NPF ranking, although to a lesser extent. For negative small ions, the concentration at around 2 nm is four to five times higher when the NPF ranking is above 0.80 compared to when it is below 0.20. For positive ions, the concentration is less than two times higher.

When looking at the small ion distributions in Beijing for different 2.0-2.3 nm ion concentrations or NPF ranking, unlike for low-volatility vapor concentrations, we are able to see the impact of growth of small ions to intermediate ions in the size distribution. In Beijing, CoagS is crucial in determining whether the growing clusters will survive to larger sizes or not, and therefore, even if the concentrations of precursors are high, growth might be negligible. A high 2.0-2.3 nm ion concentration or NPF rank means that a considerable number of clusters are able to grow without being scavenged by pre-existing larger particles.

Fig. 9b shows the scatter plots of d_{mean} and 2.0-2.3 nm ion concentration and the box plots of d_{mean} and NPF ranking. The correlation coefficients for negative ions are as expected, $r_s = 0.58$ and $r_s = 0.41$ between d_{mean} and 2.0-2.3 nm ion concentration or NPF ranking, respectively. For positive ions, the correlation coefficient between d_{mean} and NPF ranking is $r_s = 0.59$, while it is only 0.21 between d_{mean} and 2.0-2.3 nm ion concentration. From Fig. 10a we see that the concentrations of positive small ions below 1 nm also increase to some extent with increasing 2.0-2.3 nm ion concentration, which likely impacts the values of d_{mean} , resulting in a relatively poor overall correlation.

Notably, the differences in size distributions with respect to NPF ranking are clearer and the correlation between d_{mean} and ranking is stronger in Beijing than in Hyytiälä for both polarities. The explaining factors could be the fact that intense NPF in Beijing is more common than in Hyytiälä (e.g., Dada et al., 2017; Deng et al., 2020), impacting the statistics of the ranking, and that local clustering events, where ions or particles grow close to 2 nm but not much further, could be more common in Hyytiälä. Overall, our results show that compared to a rural boreal forest site like Hyytiälä, the dynamics of sub-2 nm ions in a polluted megacity like Beijing are different.

3.6 Case studies

Next, some case studies into the development of negative small ion size distributions, and other investigated variables, are presented for Hyytiälä and Beijing. These cases show that we are able to observe the cluster growth, driven by daytime NPF or evening clustering, from the ion number size distributions of individual days and not only from the statistics of the size distributions. Based on the analysis presented in this study, the behavior of negative and positive small ion populations is mostly similar, and therefore, for simplicity, we have limited the analysis here to negative polarity.



3.6.1 Hyytiälä case 1 – an early spring day with NPF

First of the investigated days was 10th of March, in 2021 and is presented in Fig. 10. During this day, a strong NPF event was observed with clear growth observed both in the total particle and ion number size distribution (see Fig. A1). In the morning, a strong increase in the SA ion dimer and trimer signals was detected after 07:00 (Fig. 10c), which occurred simultaneously with an increase in the concentration of neutral sulfuric acid. Shortly after, at around 08:00, neutral HOM monomer concentration started to increase (Fig. 10d). A strong increase in the concentration of 2.0-2.3 nm negative ions was observed after 09:00, indicating intense NPF on a local-scale (Fig. 10a). Approximately one hour before an increase in the concentration of 2.0-2.3 nm ions was first observed, the small ion d_{mean} started to increase from below 1.0 nm (Fig. 11a), showing that growth of clusters in the small ion population to larger sizes had begun. We can also see this from the negative ion number size distributions (0.8-2 nm; Fig. 10b): in the early hours of the day, the concentrations of the smallest ions are at their highest while the concentration of ions above approx. 1.1 nm are at their lowest. Throughout the morning hours, we can see that the concentration of ions above approx. 1.1 nm increases and in the afternoon, around 14:00, the concentration of ions close to 2 nm is over a order of magnitude higher than during the night before. At around 14:00, the concentration of 2.0-2.3 nm ions and small ion d_{mean} also reach their peaks. Then, the concentrations of larger small ions, 2.0-2.3 nm and SA ion clusters starts to decrease, alongside with the concentration of HOM monomers.

We also took a look at the diameter specific concentrations in a smaller time frame (Fig. A4), which clearly shows how clear increase concentrations is observed for the diameters above 1.2 nm. A time delay between the increasing concentration of larger ions and smaller ions was seen, showing the growth of ions between 1.2 to 2 nm. Using the appearance time method (Lehtipalo et al., 2014), GR between 1.24 to 2.05 nm was estimated: GR = 0.40 nm/h. This value is somewhat lower than typical GRs reported in Hyytiälä (Hirsikko et al., 2005; Yli-Juuti et al., 2011), as expected due to the small size of the considered ions. Regardless, it shows that the growth of ions below 2 nm is non-negligible.

This day clearly shows the connection between sulfuric acid and HOMs with particle formation, and illustrates how the small ion number size distribution changes as the ions grow from close to 1 nm in diameter to above 2 nm.

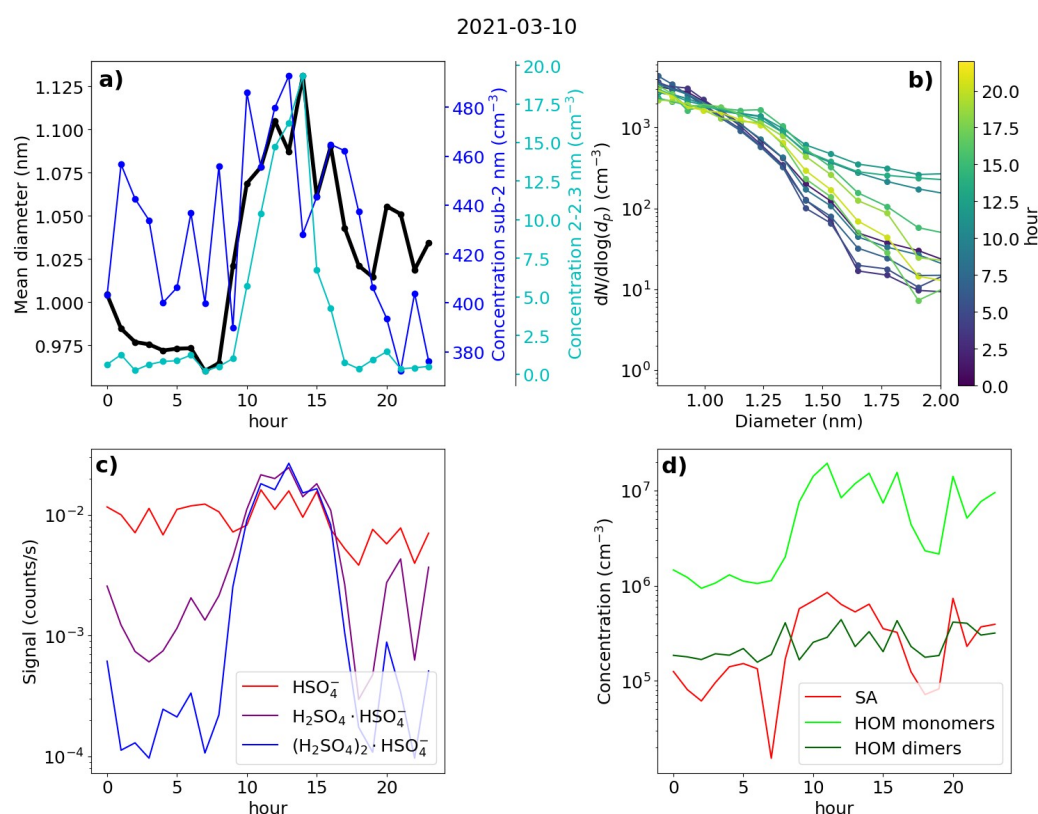


Fig. 10: Data from Hyytiälä, 10th of March, 2021. (a) Hourly mean diameter of negative small ions (0.8-2.0 nm), total concentration of small ions, and concentration of 2.0-2.3 nm negative ions. (b) Two-hour median number size distribution of negative small ions. (c) Hourly signals of HSO₄⁻, H₂SO₄·HSO₄⁻ and (H₂SO₄)₂·HSO₄⁻ ions. (d) Hourly median concentrations of neutral sulfuric acid (SA) and highly oxidized molecule (HOM) monomers and dimers.

3.6.2 Hyytiälä Case 2 – a spring day with strong evening clustering

The second of the chosen days for Hyytiälä is 19th of April, 2021 (Fig. 11). The NPF ranking of this day was high, over 0.9, however the growth in the negative ion and total particle mode was discontinuous with the clearest growth observed above 5 nm, suggesting that the fraction of growing locally formed neutral clusters or ions was low (Fig. A2). However, strong evening ion cluster formation was observed on this day. Therefore, Case 2 illustrates both the probable contribution of organic vapors to initiate the growth of larger particles and the evening ion cluster formation attributable to HOM dimers (Mazon et al., 2016).

Starting from the early hours of the day, the signals of SA ions and neutral SA concentration increase (Fig. 11c and 11d), reaching their maxima around 13:00 in the early afternoon. Compared to Hyytiälä Case 1, the signal from trimers is lower in relation to the signal from monomer and dimer. From the negative ion number size distributions (Fig. 11b), we see that the concentration of negative ions below approx. 1.2 nm increases and the concentration of small ions above approx. 1.2 nm strongly decreases starting from the early hours of the day until afternoon. This is reflected in



the value of d_{mean} , which decreases from over 1.2 nm to below 1.1 nm (Fig. 11a). The concentration of 2.0-2.3 nm negative ions decreases until 08:00 in the morning, after which it increases briefly before decreasing again (Fig. 11a). The small ion total concentration also strongly decreases from over 800 cm^{-3} to 600 cm^{-3} (Fig. 11a). Unlike in Case 1, on this day, the growth of small ions during daytime is negligible and an increased fraction of the available charge is taken up by small, below 1.2 nm ions, many of which are likely composed of sulfuric acid monomers or dimers. This explains the behavior of the ion size distributions, d_{mean} and the total small ion concentration.

After 14:00 in the afternoon, the concentration of neutral HOM dimers starts to increase, and reaches a peak at around 19:00 (Fig. 11d). Compared to Case 1, the HOM dimer concentration is over one order of magnitude higher. Notably, at the same time as the HOM dimer concentration starts increase, clear growth of total particles above 5 nm is observed (Fig. A2). Concentration of small ions larger than approx. 1.2 nm (Fig. 11b) and 2.0-2.3 nm ion concentration (Fig. 11a) strongly increase. Small ion d_{mean} increases from approx. 1.1 nm to 1.3 nm, while the total negative small ion concentration increases from around 600 cm^{-3} to 1000 cm^{-3} . The negative ion GR between 1.43 to 2.05 nm was estimated to be 1.28 nm/h (Fig. A4), which is over twice as high as the GR estimated for Case 1, likely due to the high concentration of lower volatility HOMs driving the small ion growth.

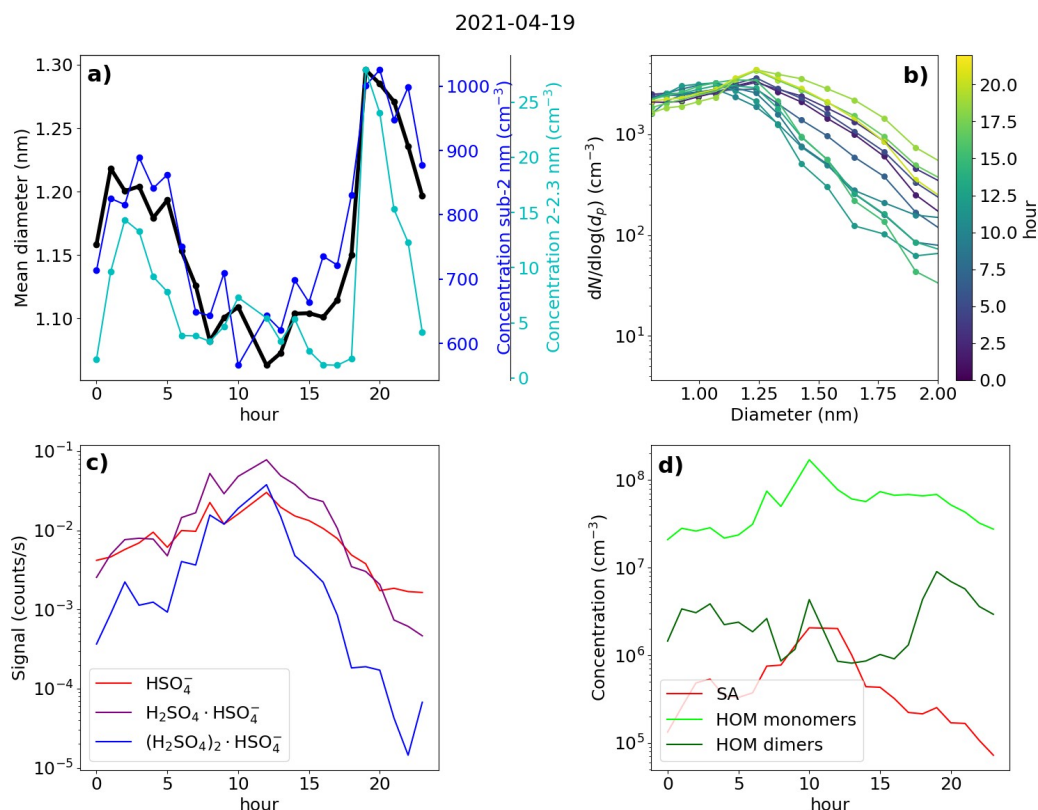


Fig. 11: Data from Hyytiälä, 19th of April, 2021. (a) Hourly mean diameter of negative small ions (0.8-2.0 nm), total concentration of small ions, and concentration of 2.0-2.3 nm negative ions. (b)

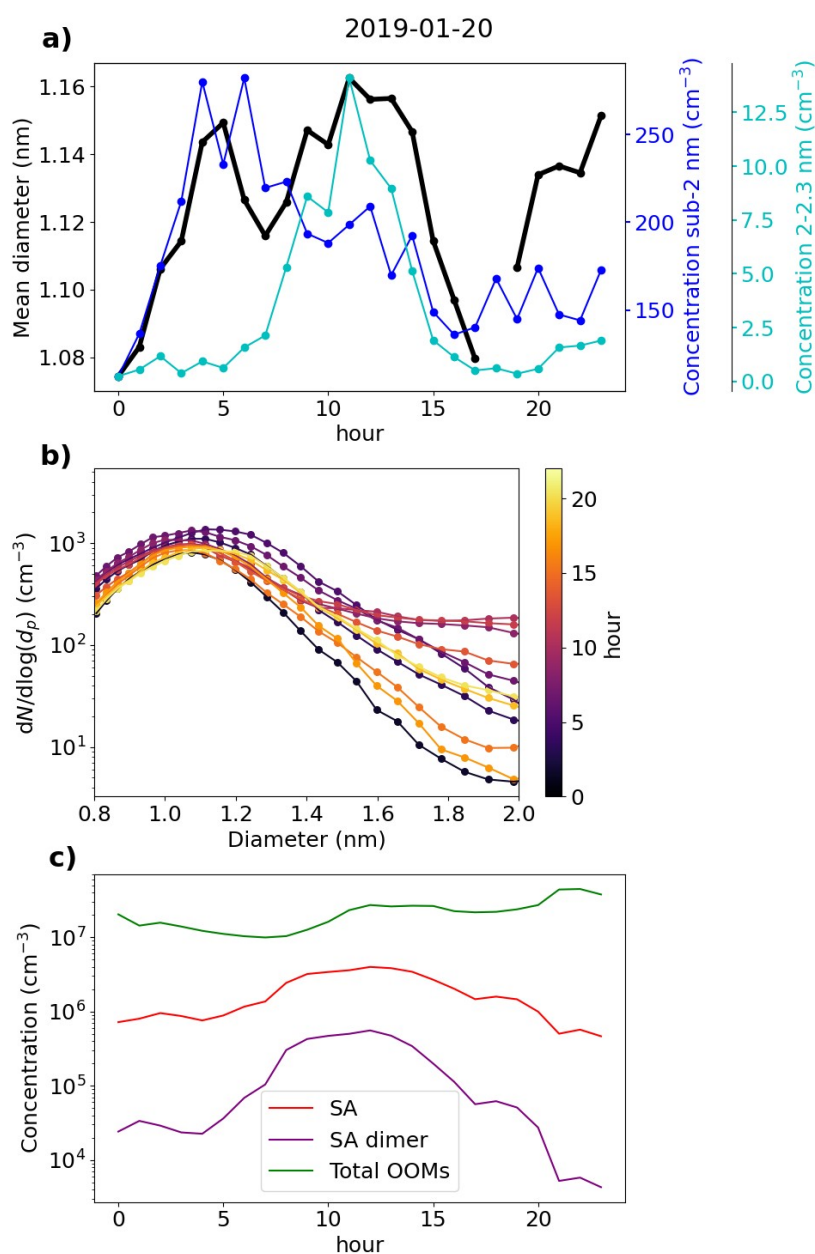


522 Two-hour median number size distribution of negative small ions. (c) Hourly signals of HSO_4^- ,
523 $\text{H}_2\text{SO}_4 \cdot \text{HSO}_4^-$ and $(\text{H}_2\text{SO}_4)_2 \cdot \text{HSO}_4^-$ ions. (d) Hourly median concentrations of neutral sulfuric acid
524 (SA) and highly oxidized molecule (HOM) monomers and dimers.

525

526 **3.6.3 Beijing Case 1 – a day with intense NPF**

527



528

529 **Fig. 12:** Data from Beijing, 20th of January, 2019. (a) Hourly mean diameter of negative small ions
530 (0.8-2.0 nm), total concentration of small ions, and concentration of 2.0-2.3 nm negative ions. (b)
531 Two-hour median number size distribution of negative small ions. (c) Hourly median concentrations
532 of neutral sulfuric acid (SA), SA dimer and total oxidized organic molecules (OOMs).

533



Fig. 12 presents data from Beijing on 20th of January, 2019. This day was characterized by an intense NPF event, observed both in the ion and total particle size distribution (Fig. A3). We see that from 00:00 until 05:00 in the morning, the negative small ion concentrations seem to increase, which is apparent for the whole sub-2 nm size range (Fig. 12a and 12b). The concentration of 2.0-2.3 nm negative ions stays low (Fig. 12a), indicating that there is no significant growth of small ions to intermediate ions. The increase in small ion concentration could be due to reduction in CS or even meteorological conditions.

After 05:00 in the morning, an increase in neutral sulfuric and sulfuric acid dimer concentration is observed (Fig. 12c). Simultaneously, the concentration of 2.0-2.3 nm ions increases sharply, indicating the formation of intermediate ions. Two changes in the small ion size distribution are shown: first, the concentration of small ions below approx. 1.5 nm ions, decreases and second, the concentration of small ions above that increases. Increasing growth of small ions to larger sizes causes a shift in their size distribution. Notably, no growth in the surface plots (Fig. A3) is observed yet, likely due to locality of or insufficient intensity of the ion formation. After 12:00, the concentrations of small ions larger than approx. 1.5 nm start to decrease, as does the concentration of 2.0-2.3 nm ions. While the growth of ions and particles at larger diameters continues, the intensity of cluster growth decreases.

In this case, the negative small ion GR was estimated to be 0.24 nm/h from 1.72 to 2.06 nm (Fig. A5), which is lower than the values determined for the two Hyytiälä cases and is on the lower range of values of particle GRs for Beijing (Deng et al., 2020). Another noteworthy observation can be made from the diameter specific concentrations (Fig. A5): as already seen from the size distributions and more clearly here, the concentrations of ions up to around 1.5 nm decrease, while the concentrations above increase at the same time. This implies that the ions, which actually start to grow to larger sizes are close to 1.5 nm in diameter, though at such a low GR their survival probability to larger sizes is likely very low (Kulmala et al., 2017).

In Sect. 3.3, we saw how in Beijing there appeared to be no correlation between the small ion number size distribution and the concentration of sulfuric acid. However, this day shows that despite the poor overall correlation, on some days there does appear to simultaneously be an increase in sulfuric acid concentration, and an increase in the growth of small ions.

4 Conclusions

We studied the seasonality of small ion number size distribution and the relationship of the small ion size distribution with low-volatility organic vapors, sulfuric acid and NPF in a rural boreal forest location of Hyytiälä, Finland and an urban megacity location of Beijing, China. Both analysis of long time series of data and daily case studies were carried out. We found a clear seasonality of the small ion size distribution in Hyytiälä, where the small ions of both polarities were the smallest in size during winter and the largest during late spring and summer. In Beijing, while there were month-to-month variations in the size distribution, but no clear seasonal pattern was identified, which we note could partly be due to the smaller number of data from Beijing compared to Hyytiälä.

We found that in Hyytiälä the small ion size distribution strongly varied with respect to the concentration of organic, especially highly oxidized organic (HOM) monomer, compounds and that



the concentration of small ions above approx. 1.2 nm increased strongly with increasing HOM monomer concentration. This was observed more strongly for negative polarity and during the evening, which was found to be connected to the evening ion cluster formation driven by organics in Hyytiälä. The small ion size distribution also showed clear increase in the size of the small ions in Hyytiälä with respect to neutral sulfuric acid and ionized sulfuric acid dimers, associated with daytime cluster formation and growth. In contrast, there was no clear relationship between the concentration of either organic vapor or sulfuric acid and the size of the small ions in Beijing. The reason for this remains to be unidentified, but we hypothesize that the high scavenging loss rate of ions could suppress or hide the impact of these vapors on the small ion size distribution.

When the concentration of ions in the range 2.0-2.3 nm increased, indicating the occurrence of local NPF, we observed clear signs of growth in the small ion size distribution. This was seen in both locations, even in Beijing, where no clear association of small ion size with organic vapor or sulfuric acid was found. To a lesser extent, an increase in the small ion size was also seen with respect to NPF rank, a parameter, which characterizes the intensity of NPF.

Overall, our results have shown in a novel way how the atmospheric cluster formation and growth processes impact the number size distribution of small ions. We have also shown how the small ion size distribution can be used to observe and get insight into these processes.

Author contributions

ST analyzed the data and wrote the manuscript. JL was responsible for the ion measurements in Hyytiälä. CL and NS were responsible for the measurements of low-volatility vapors and ion clusters. YL was responsible for the measurements in Beijing. MK and VMK conceptualized the study. All authors contributed to reviewing and editing the manuscript.

Code and data availability

The data and the codes used in the analysis and to produce the figures are available upon request from the authors.

Competing interests

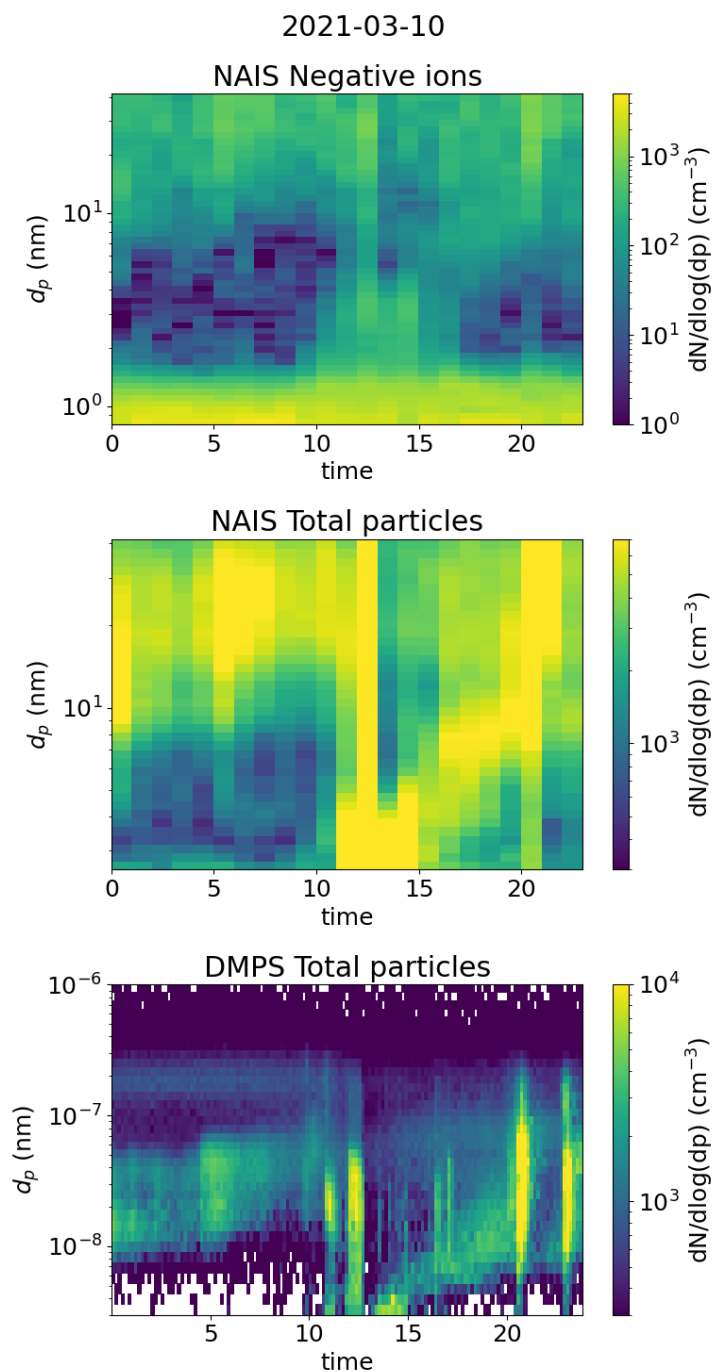
At least one of the (co-)authors is a member of the editorial board of Aerosol Research. Authors have no other competing interests to declare.

Acknowledgments

This work has been supported by the ACCC Flagship funded by the Academy of Finland grant nos. 337549 (UH) and 337552 (FMI), and the “Gigacity” project funded by the Jenny and Antti Wihuri Foundation. We acknowledge the SMEAR II and AHL/BUCT technical and scientific staff.



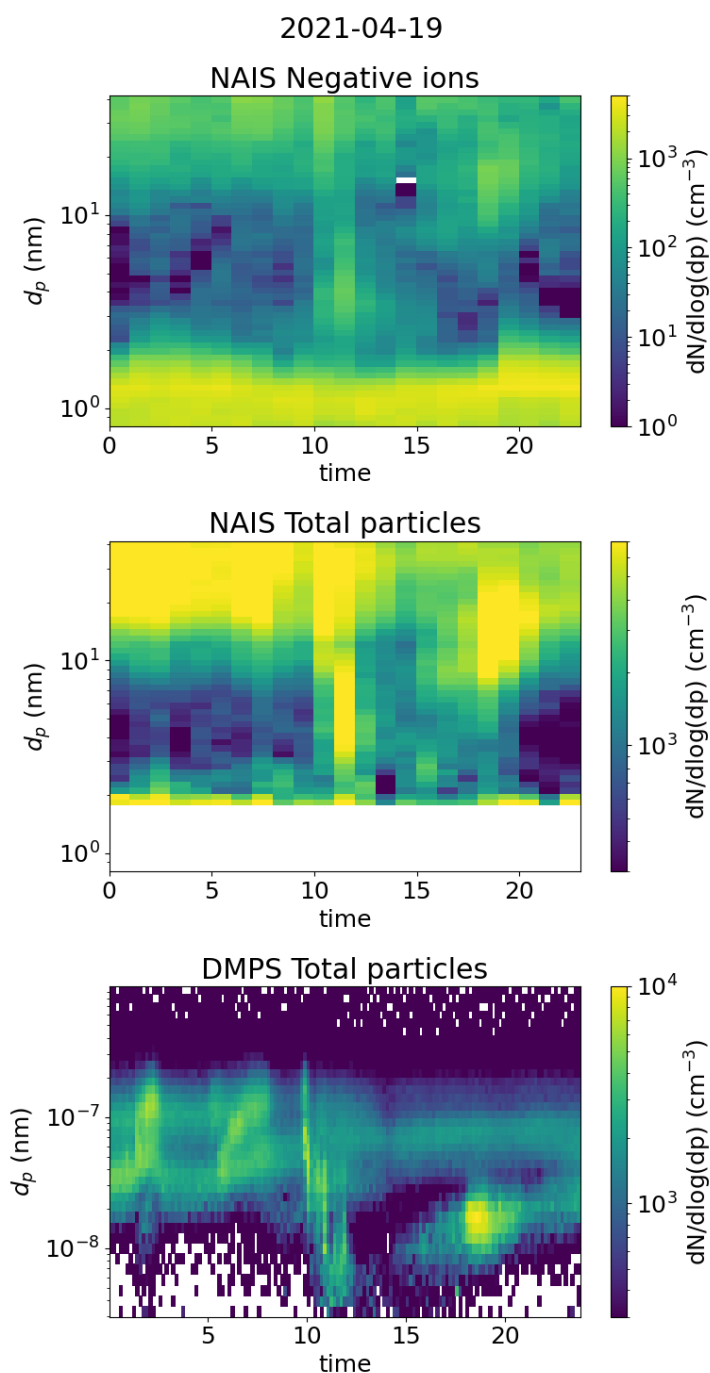
607 Appendix



608



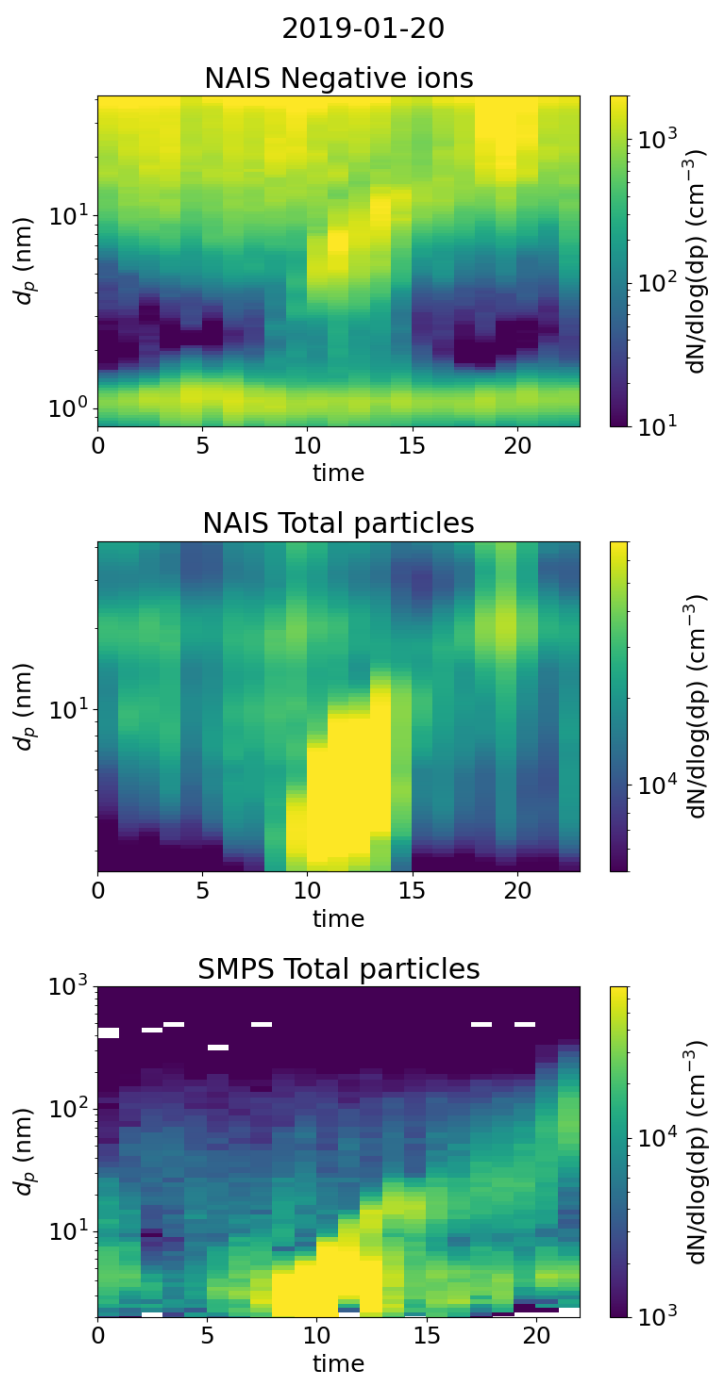
609 **Fig. A1:** Surface plots of negative ion number size distribution and total particle number size
610 distribution measured by NAIS and DMPS in Hyytiälä on 10th of March, 2021.



611



Fig. A2: Surface plots of negative ion number size distribution and total particle number size distribution measured by NAIS and DMPS in Hyytiälä on 19th of April, 2021.

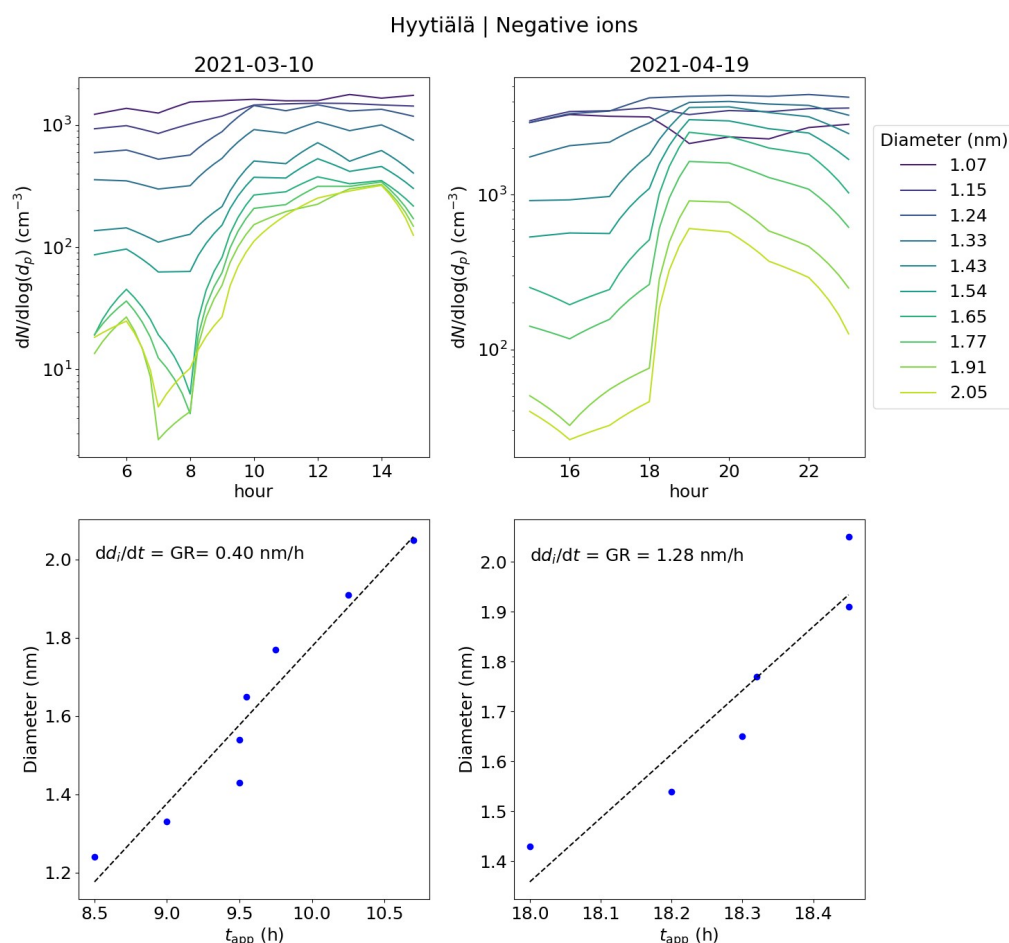


614



Fig. A3: Surface plots of negative ion number size distribution and total particle number size distribution measured by NAIS and SMPS (see Liu et al., 2016 for more information) in Beijing on 20th of January, 2019.

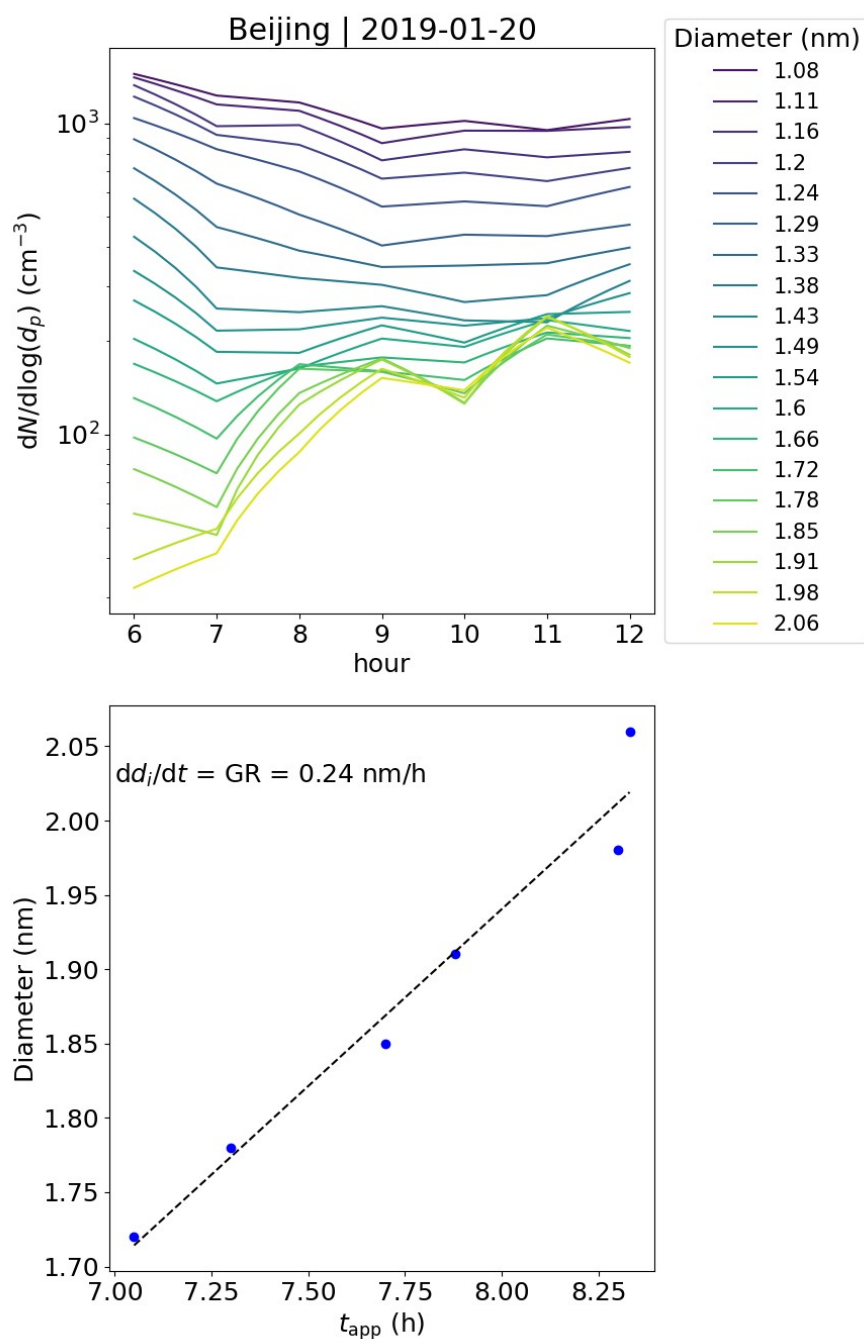
618



619

Fig. A4: The upper panels show concentrations of ions of a certain diameter with the hour of the day on 10th of March, 2021 and 19th of April, 2021 in Hyytiälä, Finland. The different colors of the line indicate the respective ion diameter (d_i). The bottom panels show the appearance time, defined as the time that the concentration reaches 50% of its maximum, and the respective d_i . The ion growth rate (GR) derived from these values as a slope of linear regression is shown. For 10th of March, the GR was determined from 1.24 to 2.05 nm and for 19th of April from 1.43 to 2.05 nm.

626



627

628 **Fig. A5:** The upper panel shows the concentrations of ions of a certain diameter with the hour of the
 629 day on 20th of January, 2019 Beijing, China. The different colors of the line indicate the respective



ion diameter (d_i). The bottom panel shows the appearance time, defined as the time that the concentration reaches 50% of its maximum, and the respective d_i . The ion growth rate (GR) derived from these values as a slope of linear regression is shown. The GR was determined from 1.72 to 2.06 nm.

References

- Aalto, P., Hämeri, K., Becker, E., Weber, R., Salm, J., Mäkelä, J. M., Hoell, C., O’ Dowd, C. D., Hansson, H.-C., Väkevä, M., Koponen, I. K., Buzorius, G., and Kulmala, M.: Physical characterization of aerosol particles during nucleation events, *Tellus B*, 53, 344–358, doi:10.1034/j.1600-0889.2001.530403.x, 2001.
- Aliaga, D., Tuovinen, S., Zhang, T., Lampilahti, J., Li, X., Ahonen, L., Kokkonen, T., Nieminen, T., Hakala, S., Paasonen, P., Bianchi, F., Worsnop, D., Kerminen, V.-M., and Kulmala, M.: Nanoparticle ranking analysis: determining new particle formation (NPF) event occurrence and intensity based on the concentration spectrum of formed (sub-5 nm) particles, *Aerosol Research*, 1, 81–92, <https://doi.org/10.5194/ar-1-81-2023>, 2023.
- Arfin, T., Pillai, A. M., Mathew, N., Tirpude, A., Bang, R., and Mondal, P.: An overview of atmospheric aerosol and their effects on human health, *Environ Sci Pollut Res* **30**, 125347–125369, <https://doi.org/10.1007/s11356-023-29652-w>, 2023.
- Atkinson, R. W., Mills, I. C., Walton, H. A., and Anderson, H. R.: Fine particle components and health—a systematic review and meta-analysis of epidemiological time series studies of daily mortality and hospital admissions. *Journal of exposure science & environmental epidemiology*, 25(2), 208–214, <https://doi.org/10.1038/jes.2014.63>, 2015.
- Bianchi, F., Garmash, O., He, X., Yan, C., Iyer, S., Rosendahl, I., Xu, Z., Rissanen, M. P., Riva, M., Taipale, R., Sarnela, N., Petäjä, T., Worsnop, D. R., Kulmala, M., Ehn, M., and Junninen, H.: The role of highly oxygenated molecules (HOMs) in determining the composition of ambient ions in the boreal forest, *Atmos. Chem. Phys.*, 17, 13819–13831, <https://doi.org/10.5194/acp-17-13819-2017>, 2017.
- Boucher, O., Randall, D., Artaxo, P., Bretherton, C., Feingold, G., Forster, P., Kerminen, V.-M., Kondo, Y., Liao, H., Lohmann, U., Rasch, P., Satheesh, S., Sherwood, S., Stevens, B., and Zhan, X.: Clouds and Aerosols, in: *Climate Change 2013: The Physical Science Basis. Contribution of Working Group I to the Fifth Assessment Report of the Intergovernmental Panel on Climate Change*, edited by: Stocker, T., Qin, D., Plattner, G., Tignor, M., Allen, S., Boschung, J., Nauels, A., Xia, Y., Bex, V., and Midgley, P., Cambridge University Press, Cambridge, United Kingdom and New York, NY, USA, 571–657, 10, <https://doi.org/10.1017/CBO9781107415324>, 2013.
- Mazon, S. B., Kontkanen, J., Manninen, H. E., Nieminen, T., Kerminen, V.-M., and Kulmala, M.: A long-term comparison of nighttime cluster events and daytime ion formation in a boreal forest, *Boreal Environ. Res.*, 21, 242–261, 2016.
- Dada, L., Paasonen, P., Nieminen, T., Buenrostro Mazon, S., Kontkanen, J., Peräkylä, O., Lehtipalo, K., Hussein, T., Petäjä, T., Kerminen, V.-M., Bäck, J., and Kulmala, M.: Long-term analysis of clear-sky new particle formation events and nonevents in Hyytiälä, *Atmos. Chem. Phys.*, 17, 6227–6241, <https://doi.org/10.5194/acp-17-6227-2017>, 2017.



- 678 Dal Maso, M., Kulmala, M., Riipinen, I., Wagner, R., Hussein, T., Aalto, P. P., and Lehtinen, K. E.
679 J.: Formation and growth of fresh atmospheric aerosols: eight years of aerosol size distribution data
680 from SMEAR II, Hyytiälä, Finland, *Boreal Environ. Res.*, 10, 323–336, 2005.
- 681
682 Deng, C., Fu, Y., Dada, L., Yan, C., Cai, R., Yang, D., Zhou, Y., Yin, R., Lu, Y., Li, X., Qiao, X.,
683 Fan, X., Nie, W., Kontkanen, J., Kangasluoma, J., Chu, B., Ding, A., Kerminen, V., Paasonen, P.,
684 Worsnop, R. D., Bianchi, F., Liu, Y., Zheng, J., Wang, L., Kulmala, M., and Jiang, J.: Seasonal
685 characteristics of new particle formation and growth in urban Beijing, *Environ. Sci. Technol.*,
686 54, 8547–8557, <https://doi.org/10.1021/acs.est.0c00808>, 2020.
- 687
688 Ehn, M., Junninen, H., Petäjä, T., Kurtén, T., Kerminen, V.-M., Schobesberger, S., Manninen, H. E.,
689 Ortega, I. K., Vehkamäki, H., Kulmala, M., and Worsnop, D. R.: Composition and temporal behavior
690 of ambient ions in the boreal forest, *Atmos. Chem. Phys.*, 10, 8513–8530, doi:10.5194/acp-10-
691 8513-2010, 2010.
- 692
693 Ehn, M., Junninen, H., Schobesberger, S., Manninen, H., Franchin, A., Sipilä, M., Petäjä, T.,
694 Kerminen, V.-M., Tammet, H., Mirme, A., Mirme, S., Hõrrak, U., Kulmala, M., and Worsnop, D.
695 R.: An instrumental comparison of mobility and mass measurements of atmospheric small ions,
696 *Aerosol Sci. Tech.*, 45, 522–532, DOI:10.1080/02786826.2010.547890, 2011.
- 697
698 Fdez-Arroyabe, P., Salcines, C., Kassomenos, P., Santurtún, A., & Petäjä, T.: Electric charge of
699 atmospheric nanoparticles and its potential implications with human health, *Science of the Total*
700 *Environment*, 808, 152106, <https://doi.org/10.1016/j.scitotenv.2021.152106>, 2022.
- 701
702 Finlay, W. H.: Deposition of aerosols in the lungs: Particle characteristics. *Journal of Aerosol*
703 *Medicine and Pulmonary Drug Delivery*, 34(4), 213–216, doi: 10.1089/jamp.2021.29040.whf,
704 2021.
- 705
706 Hari, P. and Kulmala, M.: Station for measuring ecosystem-atmosphere relations, *Boreal Environ.*
707 *Res.*, 10, 315–322, 2005.
- 708
709 Harrison, R. G. and Carslaw, K. S.: Ion-aerosol-cloud processes in the lower atmosphere, *Rev.*
710 *Geophys.*, 41(3), 1012, doi:10.1029/2002RG000114, 2003.
- 711
712 Harrison, R. G. and Tammet, H.: Ions in Terrestrial Atmosphere and Other Solar System
713 Atmospheres, *Space Sci. Rev.*, 137, 107–118, DOI 10.1007/s11214-008-9356-x, 2008.
- 714
715 Hirsikko, A., Laakso, L., Hõrrak, U., Aalto, P. P., Kerminen, V.-M. & Kulmala, M.: Annual and
716 size dependent variation of growth rates and ion concentrations in boreal forest. *Boreal Env. Res.*
717 10: 357–369, 2005.
- 718
719 Hirsikko, A., Bergman, T., Laakso, L., Dal Maso, M., Riipinen, I., Hõrrak, U., and Kulmala, M.:
720 Identification and classification of the formation of intermediate ions measured in boreal forest,
721 *Atmos. Chem. Phys.*, 7, 201–210, <https://doi.org/10.5194/acp-7-201-2007>, 2007.
- 722
723 Hirsikko, A., Nieminen, T., Gagné, S., Lehtipalo, K., Manninen, H. E., Ehn, M., Hõrrak, U.,
724 Kerminen, V.-M., Laakso, L., McMurry, P. H., Mirme, A., Mirme, S., Petäjä, T., Tammet, H.,
725 Vakkari, V., Vana, M., and Kulmala, M.: Atmospheric ions and nucleation: a review of observations,
726 *Atmos. Chem. Phys.*, 11, 767–798, <https://doi.org/10.5194/acp-11-767-2011>, 2011.
- 727



- Hörrak, U., Salm, J., and Tammet, H.: Statistical characterization of
air ion mobility spectra at Tahkuse Observatory: Classification of air ions, *J. Geophys. Res.*, 105,
9291–9302, 2000.
- Hörrak, U., Aalto, P. P., Salm, J., Komsaare, K., Tammet, H., Mäkelä, J. M., Laakso, L., and
Kulmala, M.: Variation and balance of positive air ion concentrations in a boreal forest, *Atmos.*
Chem. Phys., 8, 655–675, <https://doi.org/10.5194/acp-8-655-2008>, 2008.
- Jokinen, T., Sipilä, M., Junninen, H., Ehn, M., Lönn, G., Hakala, J., Petäjä, T., Mauldin III, R. L.,
Kulmala, M., and Worsnop, D. R.: Atmospheric sulphuric acid and neutral cluster measurements
using CI-API-TOF, *Atmos. Chem. Phys.*, 12, 4117–4125, <https://doi.org/10.5194/acp-12-4117-2012>,
2012.
- Kirkby, J., Amorim, A., Baltensperger, U., Carslaw, K. S., Christoudias, T., Curtius, J., Donahue, N.
M., Haddad, I. E., Flagan, R. C., Gordon, H., Hansel, A., Harder, H., Junninen, H., Kulmala, M.,
Kürten, A., Laaksonen, A., Lehtipalo, K., Lelieveld, J., Möhler, O., Riipinen, I., Stratmann, F.,
Tomé, A., Virtanen, A., Volkamer, R., Winkler, P. M., and Worsnop, D. R.: Atmospheric new
particle formation from the CERN CLOUD experiment, *Nat. Geosci.*, 16, 948–957,
<https://doi.org/10.1038/s41561-023-01305-0>, 2023.
- Kulmala, M., Lehtinen, K. E. J., and Laaksonen, A.: Cluster activation theory as an explanation of
the linear dependence between formation rate of 3nm particles and sulphuric acid concentration,
Atmos. Chem. Phys., 6, 787–793, <https://doi.org/10.5194/acp-6-787-2006>, 2006.
- Kulmala, M., Riipinen, I., Sipilä, M., Manninen, H., Petaja, T., Junninen, H., Dal Maso, M.,
Mordas, G., Mirme, A., Vana, M., Hirsikko, A., Laakso, L., Harrison, R., Hanson, I., Leung, C.,
Lehtinen, K., and Kerminen, V.: Toward direct measurement of atmospheric nucleation, *Science*,
318, 89–92, doi:10.1126/science.1144124, 2007.
- Kulmala, M., Petäjä, T., Nieminen, T., Sipilä, M., Manninen, H. E., Lehtipalo, K., Dal Maso, M.,
Aalto, P. P., Junninen, H., Paasonen, P., Riipinen, I., Lehtinen, K. E. J., Laaksonen, A., and
Kerminen, V.-M.: Measurement of the nucleation of atmospheric aerosol particles, *Nat. Protoc.*, 7,
1651–1667, doi:10.1038/nprot.2012091, 2012.
- Kulmala, M., Kontkanen, J., Junninen, H., Lehtipalo, K., Manninen, H. E., Nieminen, T., Petäjä, T.,
Sipilä, M., Schobesberger, S., Rantala, P., Franchin, A., Jokinen, T., Järvinen, E., Äijälä, M.,
Kangasluoma, J., Hakala, J., Aalto, P. P., Paasonen, P., Mikkilä, J., Vanhanen, J., Aalto, J., Hakola,
H., Makkonen, U., Ruuskanen, T., Mauldin, R. L., Duplissy, J., Vehkamäki, H., Bäck, J.,
Kortelainen, A., Riipinen, I., Kurtén, T., Johnston, M. V., Smith, J. N., Ehn, M., Mentel, T. F.,
Lehtinen, K. E. J., Laaksonen, A., Kerminen, V.-M., and Worsnop, D. R.: Direct Observations of
Atmospheric Aerosol Nucleation, *Science*, 339, 943–946, <https://doi.org/10.1126/science.1227385>,
2013.
- Kulmala, M., Kerminen, V. M., Petaja, T., Ding, A. J., and Wang, L.: Atmospheric gas-to-particle
conversion: why NPF events are observed in megacities?, *Faraday Discuss.*, 200, 271–288,
<https://doi.org/10.1039/c6fd00257a>, 2017.
- Kulmala M., Ezhova E., Kalliokoski T., Noe S., Vesala T., Lohila A., Liski J., Makkonen R., Bäck
J., Petäjä T. and Kerminen V.-M.: CarbonSink+ — Accounting for multiple climate feedbacks from
forests. *Boreal Env. Res.* 25: 145–159, 2020.



- 778
779 Kulmala, M., Tuovinen, S., Mirme, S., Koemets, P., Ahonen, L., Liu, Y., Junninen, H., Petäjä, T.,
780 and Kerminen, V.-M.: On the potential of the Cluster Ion Counter (CIC) to observe local new
781 particle formation, condensation sink and growth rate of newly formed particles, *Aerosol Research*,
782 2, 291–301, <https://doi.org/10.5194/ar-2-291-2024>, 2024a.
783
784 Kulmala, M., Ke, P., Lintunen, A., Peräkylä, O., Lohtander, A., Tuovinen, S., Lampilahti, J., Kolari,
785 P., Schiestl-Aalto, P., Kokkonen, T., Nieminen, T., Dada, L., Ylivinkka, I., Petäjä, T., Bäck, J.,
786 Lohila, A., Heimsch, L., Ezhova, E., and Kerminen, V. M.: A novel concept for assessing the
787 potential of different boreal ecosystems to mitigate climate change (CarbonSink+ Potential). *Boreal*
788 *Env. Res.*, 29, 1-16, 2024b.
789
790 Kulmala, M., Du, W., Zhang, X., Zhang, T., Xia, M., Wang, Y., Zou, Z., Zheng, F., Zhang, Y., Yang,
791 C., Wu, J., Li, Y., Zha, Q., Yan, C., Feng, W., Wang, Z., Hua, C., Xie, J., Ma, W., Guo, Y., Chen, X.,
792 Liu, T., Li, J., Pang, H., Zhao, G., Chen, K., Zhao, Z., Gao, S., Zhang, W., Yuan, Q., Qi, L., Petäjä,
793 T., Sarnela, N., Ylivinkka, I., Aliaga, D., Cai, R., Agro, M., Ahonen, L., Schiestl-Aalto, P.,
794 Tuovinen, S., Cai, J., Kujansuu, J., Ciarelli, G., Cheng, Y., Ding, A., Dällenbach, K., Dada, L.,
795 Worsnop, D., Bianchi, F., Jiang, J., Liu, Y., Kerminen, V.-M., Kokkonen, T.: Understanding
796 atmospheric processes: insights from the comparison between Beijing and Hyytiälä, *Npj Clean Air*
797 2025.
798
799 Lehtipalo, K., Leppä, J., Kontkanen, J., Kangasluoma, J., Franchin, A., Wimmer, D., Schobesberger,
800 S., Junninen, H., Petäjä, T., Sipilä, M., Mikkilä, J., Vanhanen, J., Worsnop, D. R., and Kulmala, M.:
801 Methods for determining particle size distribution and growth rates between 1 and 3 nm using the
802 Particle Size Magnifier, *Boreal Environ. Res.*, 19, 215–236, 2014.
803
804 Lehtipalo, K., Yan, C., Dada, L., Bianchi, F., Xiao, M., Wagner, R., Stolzenburg, D., Ahonen, L. R.,
805 Amorim, A., Baccarini, A., Bauer, P. S., Baumgartner, B., Bergen, A., Bernhammer, A.-K.,
806 Breitenlechner, M., Brilke, S., Buckholz, A., Mazon, S. B., Chen, D., Chen, X., Dias, A., Dommen,
807 J., Draper, D. C., Duplissy, J., Ehn, M., Finkenzeller, H., Fisher, L., Frege, C., Fuchs, C., Garmash,
808 O., Gordon, H., Hakala, J., He, X. C., Heikkinen, L., Heinrizi, M., Helm, J. C., Hofbauer, V., Hoyle,
809 C. R., Jokinen, T., Kangasluoma, J., Kerminen, V.-M., Kim, C., Kirkby, J., Kontkanen, J., Kürten,
810 A., Lawler, M. J., Mai, H., Mathot, S., Mauldin III, R. L., Molteni, U., Nichman, L., Nie, W.,
811 Nieminen, T., Ojdanic, A., Onnela, A., Passananti, M., Petäjä, T., Piel, F., Pospisilova, V.,
812 Quéléver, L. L. J., Rissanen, M. P., Rose, C., Sarnela, N., Schallhart, S., Sengupta, K., Simon, M.,
813 Tauber, C., Tomé, A., Tröst, J., Väisänen, O., Voge, A. L., Volkamer, R., Wagner, A. C., Wang, M.,
814 Weitz, L., Wimmer, D., Ye, P., Ylisirniö, A., Zha, Q., Carslaw, K., Curtius, J., Donahue, N., Flagan,
815 R. C., Hansel, A., Riipinen, I., Virtanen, A., Winkler, P. M., Baltensperger, U., Kulmala, M., and
816 Worsnop, D. R.: Multi-component new particle formation from sulfuric acid, ammonia and biogenic
817 vapors, *Sci. Adv.*, 4, eaau5363, <https://doi.org/10.1126/sciadv.aau5363>, 2018.
818
819 Li, J., Carlson, B. E., Yung, Y. L., Lv, D., Hansen, J., Penner, J. E., Liao, H., Ramaswamy, V., Kahn,
820 R. A., Zhang, P., Dubovik, O., Ding, A., Lacis, A. A., Zhang, L., and Dong, Y.: Scattering and
821 absorbing aerosols in the climate system, *Nature Reviews Earth & Environment*, 3, 363–379,
822 <https://doi.org/10.1038/s43017-022-00296-7>, 2022.
823
824 Liu, J. Q., Jiang, J. K., Zhang, Q., Deng, J. G., and Hao, J. M.: A spectrometer for measuring
825 particle size distributions in the range of 3 nm to 10 μ m, *Front. Env. Sci. Eng.*, 10, 63–72,
826 <https://doi.org/10.1007/s11783-014-0754-x>, 2016.
827



- 828 Liu, Y., Yan, C., Feng, Z., Zheng, F., Fan, X., Zhang, Y., Li, C., Zhou, Y., Lin, Z., Guo, Y., Zhang,
829 Y., Ma, L., Zhou, W., Liu, Z., Dada, L., Dällenbach, K., Kontkanen, J., Cai, R., Chan, T., Chu, B.,
830 Du, W., Yao, L., Wang, Y., Cai, J., Kangasluoma, J., Kokkonen, T., Kujansuu, J., Rusanen, A., Deng,
831 C., Fu, Y., Yin, R., Li, X., Lu, Y., Liu, Y., Lian, C., Yang, D., Wang, W., Ge, M., Wang, Y., Worsnop,
832 D. R., Junninen, H., He, H., Kerminen, V.-M., Zheng, J., Wang, L., Jiang, J., Petäjä, T., Bianchi, F.,
833 and Kulmala, M.: Continuous and comprehensive atmospheric observations in Beijing: a station to
834 understand the complex urban atmospheric environment, *Big Earth Data*, 4, 295–321,
835 <https://doi.org/10.1080/20964471.2020.1798707>, 2020
836
837 Mirme, S. and Mirme, A.: The mathematical principles and design of the NAIS – a spectrometer for
838 the measurement of cluster ion and nanometer aerosol size distributions, *Atmos. Meas. Tech.*, 6,
839 1061–1071, <https://doi.org/10.5194/amt-6-1061-2013>, 2013.
840
841 Mirme, S., Balbaaki, R., Manninen, H. E., Koemets, P., Sommer, E., Rörup, B., Wu, Y., Almeida, J.,
842 Ehrhart, S., Weber, S. K., Pfeifer, J., Kangasluoma, J., Kulmala, M., and Kirkby, J.: Design and
843 performance of the Cluster Ion Counter (CIC), *Atmos. Meas. Tech. Discuss.* [preprint],
844 <https://doi.org/10.5194/amt-2024-138>, accepted for publication, 2024.
845
846 Quaas, J., Ming, Y., Menon, S., Takemura, T., Wang, M., Penner, J.E., Gettelman, A., Lohmann, U.,
847 Bellouin, N., Boucher, O., Sayer, A.M., Thomas, G.E., McComiskey, A., Feingold, G., Hoose, C.,
848 Kristjánsson, J.E., Liu, X., Balkanski, Y., Donner, L. J., Ginoux, P.A., Stier, P., Grandey, B.,
849 Feichter, J., Sednev, I., Bauer, S.E., Koch, D., Grainger, R.G., Kirkevåg, A., Iversen, T., Seland, Ø.,
850 Easter, R., Ghan, S.J., Rasch, P.J., Morrison, H., Lamarque, J.-F., Iacono, M. J., Kinne, S., and
851 Schulz, M.: Aerosol indirect effects – general circulation mode intercomparison and evaluation with
852 satellite data, *Atmos. Chem. Phys.*, 9, 8697–8717, doi:10.5194/acp-9-8697-2009, 2009.
853
854 Rose, C., Zha, Q., Dada, L., Yan, C., Lehtipalo, K., Junninen, H., Mazon, S. B., Jokinen, T., Sarnela,
855 N., Sipilä, M., Petäjä, T., Kerminen, V.-M., Bianchi, F., and Kulmala, M.: Observations of biogenic
856 ion-induced cluster formation in the atmosphere, *Sci. Adv.*, 4, 1–11, DOI:[10.1126/sciadv.aar5218](https://doi.org/10.1126/sciadv.aar5218),
857 2018.
858
859 Schmale, J., Zieger, P., and Ekman, A. M. L.: Aerosols in current and future Arctic climate, *Nat.*
860 *Clim. Change*, 11, 95–105, <https://doi.org/10.1038/s41558-020-00969-5>, 2021.
861
862 Shiraiwa, M., Ueda, K., Pozzer, A., Lammel, G., Kampf, C. J., Fushimi, A., Enami, S., Arangio, A.
863 M., Fröhlich-Nowoisky, J., Fujitani, Y., Furuyama, A., Lakey, P. S. J., Lelieveld, J., Lucas, K.,
864 Morino, Y., Pöschl, U., Takahama, S., Takami, A., Tong, H., Weber, B., Yoshino, A., and Sato, K.:
865 Aerosol health effects from molecular to global scales, *Environ. Sci. Technol.*, 51, 13545–13567,
866 <https://doi.org/10.1021/acs.est.7b04417>, 2017.
867
868 Shuman, N. S., Hunton, D. E., and Viggiano, A. A.: Ambient and modified atmospheric ion
869 chemistry: from top to bottom, *Chem. Rev.*, 115, 4542–4570, <https://doi.org/10.1021/cr5003479>,
870 2015.
871
872 Sulo, J., Sarnela, N., Kontkanen, J., Ahonen, L., Paasonen, P., Laurila, T., Jokinen, T.,
873 Kangasluoma, J., Junninen, H., Sipilä, M., Petäjä, T., Kulmala, M., and Lehtipalo, K.: Long-term
874 measurement of sub-3 nm particles and their precursor gases in the boreal forest, *Atmos. Chem.*
875 *Phys.*, 21, 695–715, <https://doi.org/10.5194/acp-21-695-2021>, 2021.
876



877 Tammet, H.: Size and mobility of nanometer particles, clusters and ions, *J. Aerosol Sci.*, 26, 459–
878 475, 1995.

879

880 Tammet, H., Hörrak, U., Laakso, L., and Kulmala, M.: Factors of air ion balance in a coniferous
881 forest according to measurements in Hyytiälä, Finland, *Atmos. Chem. Phys.*, 6, 3377–3390,
882 <https://doi.org/10.5194/acp-6-3377-2006>, 2006.

883

Tammet, H., Komsaare, K., and Horrak, U.: Intermediate ions in the atmosphere, *Atmos. Res.*, 135–
136, 263–273, <https://doi.org/10.1016/j.atmosres.2012.09.009>, 2014.

Tuovinen, S., Lampilahti, J., Kerminen, V.-M., and Kulmala, M.: Intermediate ions as indicator for
local new particle formation, *Aerosol Research*, 2, 93–105, <https://doi.org/10.5194/ar-2-93-2024>,
2024.

Wagner, R., Manninen, H. E., Franchin, A., Lehtipalo, K., Mirme, S., Steiner, G., Petäjä, T., and
Kulmala, M.: On the accuracy of ion measurements using a Neutral cluster and Air Ion
Spectrometer, *Boreal Env. Res.*, 21, 230–241, 2016

Yan, C., Yin, R., Lu, Y., Dada, L., Yang, D., Fu, Y., Kontkanen, J., Deng, C., Garmash, O., Ruan, J.,
Baalbaki, R., Schervish, M., Cai, R., Bloss, M., Chan, T., Chen, T., Chen, Q., Chen, X., Chen, Y.,
Chu, B., Dällenbach, K., Foreback, B., He, X., Heikki-nen, L., Jokinen, T., Junninen, H.,
Kangasluoma, J., Kokkonen, T., Kurppa, M., Lehtipalo, K., Li, H., Li, H., Li, X., Liu, Y., Ma, Q.,
Paasonen, P., Rantala, P., Pileci, R. E., Rusanen, A., Sarnela, N., Simonen, P., Wang, S., Wang, W.,
Wang, Y., Xue, M., Yang, G., Yao, L., Zhou, Y., Kujansuu, J., Petäjä, T., Nie, W., Ma, Y., Ge, M.,
He, H., Donahue, N. M., Worsnop, D. R., Veli-Matti, K., Wang, L., Liu, Y., Zheng, J., Kulmala, M.,
Jiang, J., and Bianchi, F.: The Synergistic Role of Sulfuric Acid, Bases, and Oxidized Organics
Governing New-Particle Formation in Beijing, *Geophys. Res. Lett.*, 48, e2020GL091944,
<https://doi.org/10.1029/2020gl091944>, 2021.

Yli-Juuti, T., Nieminen, T., Hirsikko, A., Aalto, P. P., Asmi, E., Hörrak, U., Manninen, H. E.,
Patokoski, J., Dal Maso, M., Petäjä, T., Rinne, J., Kulmala, M., and Riipinen, I.: Growth rates of
nucleation mode particles in Hyytiälä during 2003–2009: variation with particle size, season, data
analysis method and ambient conditions, *Atmos. Chem. Phys.*, 11, 12865–12886,
<https://doi.org/10.5194/acp-11-12865-2011>, 2011.

884

885

886

887